geosciences

MDPI

Article

Advanced GIS-Based RUSLE Modeling for Soil Erosion Estimation in the Toplica River Basin, Serbia

Milan Đorđević [1,*], Mrđan Đokić [1], Miloš Manić [2], Jelena Vesković [3], Ranko Dragović [1], Ivana Smičiklas [4], Snežana Dragović [4] and Antonije Onjia [3]

[1] Department of Geography and Tourism, Faculty of Sciences and Mathematics, University of Niš, Višegradska 33, 18000 Niš, Serbia; mrdjan.djokic@pmf.edu.rs (M.Đ.); ranko.dragovic@pmf.edu.rs (R.D.)
[2] Faculty of Geography, University of Belgrade, Studentski Trg 3, 11000 Belgrade, Serbia; dd18011@studenti.gef.bg.ac.rs
[3] Faculty of Technology and Metallurgy, University of Belgrade, Karnegijeva 4, 11120 Belgrade, Serbia; jveskovic@tmf.bg.ac.rs (J.V.); onjia@tmf.bg.ac.rs (A.O.)
[4] "VINČA" Institute of Nuclear Sciences—National Institute of the Republic of Serbia, University of Belgrade, Mike Petrovića Alasa 12–14, 11351 Belgrade, Serbia; ivanat@vin.bg.ac.rs (I.S.); sdragovic@vin.bg.ac.rs (S.D.)
* Correspondence: milan.djordjevic@pmf.edu.rs; Tel.: +381-66005474

Abstract

Among the most serious types of land degradation, soil erosion poses a major threat to agricultural productivity, water quality, and ecosystem stability. Using a multidisciplinary approach, this study aimed to identify the spatial patterns of soil erosion and dominant drivers influencing soil loss in the Toplica River Basin in southern Serbia. Soil properties, including texture and organic matter content, were analyzed in samples collected throughout the study area, accounting for variations in altitude, soil type, and land use, to determine the erodibility factor (K). The rainfall erosivity factor (R), topographic factor (LS), and cover management factor (C) were determined using available inputs on rainfall erosivity, topography, land use, and vegetation cover. The Revised Universal Soil Loss Equation (RUSLE) was used to estimate annual soil erosion rates, and GIS tools and cartographic techniques were used to create spatial layers for each RUSLE factor and to generate a detailed erosion risk map. The results showed a mean annual soil loss of 5.45 t ha^{-1} $year^{-1}$, with values ranging from 0 to 397.09 t ha^{-1} $year^{-1}$, indicating considerable spatial variability. The regression modeling revealed the dominant roles of factors LS ($\beta = 0.828$), C ($\beta = 0.731$), and their interaction (LS × C, $\beta = 0.561$), followed by rainfall-related interactions (R × C, $\beta = 0.268$ and R × LS, $\beta = 0.261$). Two dominant erosion regimes were distinguished: topography-controlled erosion in mountainous regions and land-use-controlled erosion in low- to moderately sloping agricultural areas. The maps and analyses presented in this study provide a process-based framework for interpreting spatial erosion patterns, identifying critical hotspots and areas with higher erosion risk, and supporting more focused and context-aware conservation strategies.

Keywords: K-factor; land use impact; susceptibility mapping; rainfall erosivity; watershed; soil texture

Check for updates

Received: 29 November 2025
Revised: 5 February 2026
Accepted: 10 February 2026
Published: 14 February 2026

Copyright: © 2026 by the authors. Licensee MDPI, Basel, Switzerland. This article is an open access article distributed under the terms and conditions of the Creative Commons Attribution (CC BY) license.

1. Introduction

Sustainably managed fertile soil is essential for agriculture and for meeting future human needs, including food production, livestock feed, and access to clean water [1–4]. Given that healthy soils provide significant ecosystem services [5–7], close collaboration

between scientists and policymakers is crucial for achieving sustainable development goals and enhancing the overall well-being of communities.

Among the causes of land degradation worldwide, soil erosion is one of the most significant, as it disrupts essential ecosystem functions, reduces biological diversity, limits agricultural output, and depletes soil organic carbon stocks. These negative impacts further contribute to broader environmental issues, including climate change, deterioration of water quality, and a decline in ecosystem resilience [8–12].

European soil functionality, crop production, and water quality are largely threatened by water-driven soil erosion [8]. This natural process is particularly intensified in areas where land use has been changed, leading to a loss of natural vegetation. Each year, significant amounts of fertile soil are lost to erosion, degrading millions of hectares of productive land and severely impacting agricultural productivity [13–15]. Erosion processes, their distribution, and timing are closely linked to anthropogenic factors, such as local social, economic, and demographic conditions [16]. Demographic factors, including population growth, density, and age structure, are key factors in shaping land use practices and, consequently, influence erosion dynamics [17–20]. Studies have demonstrated that demographic changes, including population decline and aging, lead to land abandonment and reduced agricultural activity, subsequently decreasing erosion intensity [21–24]. Conversely, intensified land use frequently elevates erosion risk in areas with stable or increasing populations. The reduction or loss of protective land cover increases soil exposure to rainfall and surface runoff, thereby enhancing its susceptibility to erosion [25].

The study of water soil erosion is supported by a wide range of methodological approaches, among which empirical methods are the most commonly applied [26,27]. Empirical models are based on statistical relationships derived from observed erosion data and are frequently used for large-scale assessments due to their simplicity and low data demand [10,28,29]. Among them, the Universal Soil Loss Equation (USLE), developed by Wischmeier and Smith (1978) [30], and its modified versions, such as the Revised Universal Soil Loss Equation (RUSLE) developed by Renard et al. (1997) [31], have been extensively applied worldwide. RUSLE accounts for environmental conditions such as relief, climate, soil properties, and human influence, incorporating factors like rainfall erosivity (R), soil erodibility (K), slope length and steepness (LS), cover-management (C), and support practices (P) to estimate the average annual soil loss resulting from interrill and rill erosion.

According to the study by Pandey et al. (2021) [32], which reviewed 160 scientific papers on soil erosion vulnerability assessment published between 1991 and 2019, RUSLE was identified as the most widely used model, applied in 42.7% of the analyzed studies, reflecting its broad acceptance and applicability across diverse geographical settings. Benavidez et al. (2018) [33] and Alewell et al. (2019) [34] also highlighted that USLE and its modifications, including RUSLE, which have a long history of use for assessing soil erosion worldwide, remain the most widely applied approaches. The popularity of RUSLE is attributed to its simplicity, adaptability, minimal data requirements, and applicability in different environments [35–38]. Advances in GIS and remote sensing have further improved the predictive capabilities of RUSLE, allowing more accurate spatial modeling of erosion potential [16].

Although RUSLE was initially developed for sheet and rill erosion on farms, it has also proven helpful for larger-scale assessments at national and continental scales [39]. Its suitability for national-scale assessments is supported by several factors: the availability of soil, topographic, climatic, and vegetation datasets, the efficient processing of large amounts of data through GIS integration, extensive scientific literature for regional compar-

isons, and the ability to assess both current erosion patterns and potential future climate change impacts [40].

The issue of water-induced soil erosion has been extensively addressed by the European Environment Agency (EEA) and the Joint Research Centre (JRC) of the European Commission [41], emphasizing the spatial distribution and environmental impacts of erosion across the European Union. Panagos et al. (2020) [42] estimated the mean soil erosion rate in the EU to be 2.45 t ha^{-1} $year^{-1}$ in 2016, which is nearly identical to the 2010 value of 2.46 t ha^{-1} $year^{-1}$, indicating a marginal decline of 0.4% over six years. A more pronounced 9% reduction was observed during the period from 2000 to 2010.

While considerable efforts have been made across much of Europe to quantify soil loss and identify erosion-prone areas, comprehensive assessments remain lacking in some regions. In recent decades, USLE and RUSLE have been applied in Serbia and neighboring countries to estimate erosion intensity and support land management planning. However, their application has typically been limited to river catchments or municipal territories, and large-scale assessments remain scarce. In Serbia, previous studies have applied the USLE and RUSLE models to specific areas, including the Bačka region, northern Serbia [43], the Kolubara District [44], and the Crveni Potok watershed in eastern Serbia [45]. Several studies by Perović and collaborators focused on eastern Serbia, including the municipality of Pirot [46], the mountainous Nišava watershed [38], and the municipality of Niš [47]. Similarly, Životić et al. (2012) [48] explored the application of USLE in southeastern Serbia, combining GIS and remote sensing. In the wider region, RUSLE has been used to assess erosion potential in the Republic of Srpska (BiH) [49] and across Romania [50].

Although previous studies have significantly advanced our understanding of soil erosion across various parts of Serbia, many regions remain unassessed by erosion modeling.

The aim of this study was to assess the spatial pattern and relative variability of erosion susceptibility in an environmentally and economically important but insufficiently studied region of southern Serbia. By integrating soil characterization, GIS-based RUSLE modeling, and erosion factor analysis, the research provides novel insights into soil erosion dynamics within the Toplica River Basin and directs soil conservation planning by identifying priority erosion hotspots. The main objectives of this research were to: (1) analyze the overall state of erosion within the Toplica River Basin to evaluate the extent and spatial distribution of erosion processes; (2) identify the most erosion-prone areas and explore the key factors driving high erosion rates; (3) determine the dominant erosion factors and assess their relative significance across different parts of the watershed; (4) investigate potential interactions among erosion factors to identify critical combinations that substantially contribute to erosion intensity; (5) evaluate the findings by comparing them with similar erosion studies conducted in Serbia and worldwide, and (6) contribute to filling gaps on the European soil erosion map.

2. Study Area

The study area encompasses the Toplica River Basin, with its western boundary defined by the eastern slopes of Kopaonik Mountain, a prominent mountain ridge in the southern Serbia (Figure 1). The basin is part of the Južna Morava River system, and the Toplica River represents its largest left-bank tributary. Kopaonik extends in a meridional direction, with its main ridge directing precipitation runoff from the eastern slopes toward the Toplica River. To the north, the basin is bordered by Veliki Jastrebac Mountain, while Radan Mountain forms the southern boundary. In contrast, the eastern side of the basin lacks a distinct morphological barrier, allowing the Toplica River to flow freely toward its confluence with the Južna Morava. Geotectonically and morphostructurally, the study area predominantly belongs to the Serbo-Macedonian Massif and, in its western part, to the

Inner Dinarides, particularly to the structural framework of the Kopaonik Block. Some transitional features also indicate influence from the adjacent Vardar Zone. The Serbo-Macedonian Massif was uplifted during the Hercynian orogeny, while the Dinarides were formed during the Alpine orogeny.

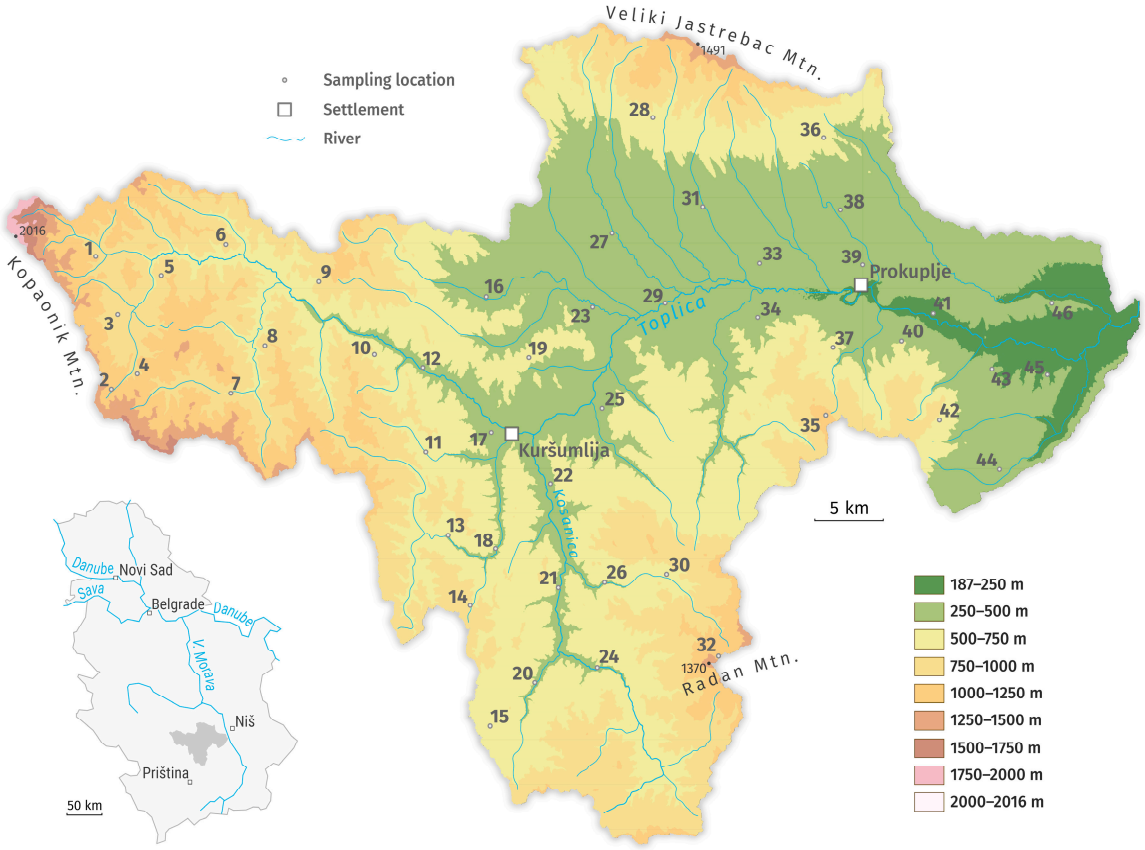


Figure 1. The Toplica River Basin and its geographical location in Serbia (red dots represent the locations of sampling points).

The relief of the Toplica River Basin includes hilly and mountainous landscapes with diverse morphological characteristics and elevation zones. The total basin area is approximately 2197 km^2, with an elevation difference of over 1800 m between the highest point in the west, on Kopaonik Mountain (2017 m), and the lowest point near its confluence with the Južna Morava River (approximately 187 m above sea level). The average elevation of the basin is 632 m above sea level, with lacustrine sedimentation and fluvial erosion and sedimentation during the Quaternary period.

The geological structure of the Toplica River Basin is complex, resulting from the interplay of rock formations of different ages, lacustrine phases, fluvial processes, and tectonic activity. In the western part of the basin, on the slopes of Kopaonik Mountain, the geological structure includes various types of igneous rocks of different ages, ranging from the Paleozoic to the Miocene and Pliocene, as well as sandstones, conglomerates, breccias, siltstones, and marlstones of Cretaceous age. Endogenous tectonic processes during the Tertiary shaped the primary morphostructural forms of Kopaonik Mountain, which were later modified by exogenous forces during regression and uplift. Moving eastward, the mountainous terrain is predominantly composed of ancient Paleozoic metamorphic rocks, but includes igneous formations of varying ages, primarily from the Oligocene and Miocene. In the northern part of the basin, on Jastrebac Mountain, the terrain consists of different schists and metamorphosed gabbros, with sporadic occurrences of igneous rocks, particularly gneiss-granites. The southern part of the basin is characterized by widespread

occurrences of andesites and pyroclastic rocks, along with clastic rocks composed of volcanic material (tuff, tuffaceous gravel, breccia). The lower parts of the basin, particularly north of the Toplica River, are composed of Miocene lacustrine sediments consisting of gravel, siltstones, clays, and claystones. In this section of the basin, the area along the river is built upon alluvium, above which river terraces rise. Towards Jastrebac Mountain, lacustrine sediments transition into unsorted proluvial and deluvial deposits, transported by mountain streams [51,52]. Due to the basin's lithological and hydrogeological characteristics, water retention above the erosion base is minimal, resulting in rapid surface runoff during periods of increased precipitation and reduced flow during dry periods [51].

The complex geological structure, intricate climatic characteristics, and associated natural vegetation significantly influence the high diversity of soil types within the Toplica River Basin. In the mountainous areas, where the geological substrate consists of metamorphic and igneous rocks, Vertic Cambisols (Eutric) and Vertic Cambisols (Dystric) are most commonly found, along with Haplic Cambisols (Eutric), Umbric Leptosols (Dystric), and Podzols. Vertic Cambisols (Eutric) are predominantly developed on lacustrine sediments, although smaller areas also exhibit Haplic Cambisols (Eutric). Along rivers, in fluvial deposits, the most prevalent soils are Haplic Fluvisols (Eutric), with less frequent Haplic Fluvisols (Calcaric) [52].

From a biogeographical perspective, Kopaonik Mountain exemplifies the altitudinal vegetation stratification within the northern temperate climatic zone. Vegetation composition is influenced by edaphic factors, regional climatic circulation, and the meridional orientation of the mountain massif. Approximately 1600 plant species have been recorded on Kopaonik, of which 825 belong to the high-mountain flora [53]. These factors cause local differences in vegetation composition between the northern and southern slopes, as well as between the eastern and western sides, separated by the main mountain ridge. The lowest vegetation zone consists of mixed deciduous forests dominated by oak species (Quercus). Thermophilous oak forests occupy the submontane and lower montane belts up to approximately 800 m a.s.l. Above this zone, forests of Sessile oak (Quercus petraea) and Turkey oak (Quercus cerris). In the northern part of Kopaonik Mountain, stands of Balkan beech (Fagetum moesiacae submontanum) are present [54].

Historically, Kopaonik was known for extensive spruce (Picea) forests on podzolic soils. Today, these forests are largely preserved only in fragmented patches within Kopaonik National Park [53], while illegal logging and insufficient regeneration in unprotected areas continue to disrupt the natural cycle. The consequences of deforestation and forest degradation are significant for soil stability, as the removal of vegetation and root systems leaves relatively young soils exposed and prone to erosion. Some stands have also been affected by drought-induced tree mortality, caused by regional climate changes and uneven summer precipitation.

The Toplica River Basin lies within the moderate continental climate zone. Precipitation is the most important climatic factor influencing erosion processes. This basin is among the driest regions in Serbia. At the meteorological station in Kuršumlija, located in the basin's central part, average annual precipitation is approximately 650 mm. At higher elevations, precipitation increases, exceeding 900 mm at the highest peaks of Kopaonik Mountain. Precipitation is relatively evenly distributed throughout the year, with a maximum from May to July (60–66 mm per month) and a minimum in August (42 mm), January (42 mm), and February (45 mm). A substantial snowpack accumulates in the mountainous areas during winter and melts in spring. Snow cover persists for a particularly long time on Kopaonik, averaging over five months per year. This snowmelt often coincides with peak rainfall, significantly increasing runoff volumes and surface water erosion [55].

3. Materials and Methodology

3.1. Sampling Approach

Soil samples were collected at 46 locations (Figure 1; Table A1) distributed throughout the basin. The sampling points were not laid out on a regular grid; rather, a stratified random sampling design was used to ensure all major sub-regions and land uses within the basin were represented. This allowed us to capture the spatial variability of soil properties across the study area. The sampling included sites under forest (18 sites; 39%), grassland (22 sites; 48%), and agricultural land use (6 sites; 13%), to ensure representativeness across the basin's main land cover categories. In terms of lithology, the sampling points were distributed across consolidated sedimentary rocks (23 sites; 50.0%), magmatic rocks (10 sites; 21.7%), metamorphic rocks (8 sites; 17.4%), and unconsolidated Quaternary sediments (5 sites; 10.9%), thereby covering the principal geological units that influence soil formation and erosion processes. One composite soil sample was collected at each location from the 0–30 cm depth interval with an auger (Eijkelkamp, Giesbeek, The Netherlands). The disturbed soil samples were immediately placed in labeled plastic bags and sealed to prevent moisture loss or loss of fine soil particles during transport. To determine soil dry bulk density (BD), undisturbed samples were collected using standard steel core rings (5 cm height × 5 cm diameter, 100 cm^3). The cylinders were carefully extracted from the soil to prevent soil loss or changes in the sample structure. Sampling points were positioned using a GPS device (TDC100 GPS, Trimble GmbH, Raunheim, Germany).

3.2. Soil Analysis

Soil samples collected from the study area were analyzed for key properties influencing water erosion, including dry bulk density (BD), particle size distribution and coarse fraction content, total organic carbon (TOC), soil structure class (S), and soil permeability (P), with detailed values for each sampling location provided in Table A1. Prior to texture analysis, the soil was sieved at 2 mm to remove the coarse fraction (particles > 2 mm diameter). The remaining fine-earth fraction (<2 mm) was then used for particle size distribution determination.

3.2.1. Dry Bulk Density (BD)

The soil's dry bulk density (BD) was determined using the Kopecky core method in accordance with the international standard [56]. The samples were dried at 105 °C to a constant weight.

3.2.2. Determination of Particle Size Distribution and Skeletal Content

The determination of the granulometric composition and skeletal content of the soil was conducted according to the standard [57]. The soil samples were first dried to a constant weight to remove moisture and then sieved through a 2 mm mesh to separate the skeletal material from the fine fraction. The skeletal content was expressed as a percentage by mass relative to the sample's total mass. Organic matter was removed by adding hydrogen peroxide and heating, while carbonates were eliminated by adding a hydrochloric acid solution. Sand fractions, including fine sand (0.05–0.1 mm) and medium to coarse sand (0.1–2.0 mm), were determined by sieving through a series of appropriately sized sieves, while silt (0.002–0.05 mm) and clay (<0.002 mm) fractions were separated by sedimentation.

3.2.3. Total Organic Carbon (TOC)

The organic carbon content was determined in accordance with ISO 14235:1998 [58], a widely used standard in soil research due to its accuracy and simplicity. The water content in the samples, expressed as a percentage of dry mass, was determined according to ISO

11465:1993 [59]. A Lambda 40 spectrophotometer (Perkin Elmer, MA, USA) was used for the spectrophotometric determination of organic carbon. To ensure the accuracy and precision of the results, control samples with known organic carbon content were analyzed, along with blank samples, to eliminate contamination-related measurement errors. Each measurement was performed in triplicate on the same soil sample, and the three results were averaged.

3.2.4. Soil Structure Class (s)

The soil structure class was determined using data from the European Soil Data Centre [60]. The classification was based on pedological parameters, including soil type according to the Food and Agriculture Organization (FAO) classification [61] and soil texture. Based on these characteristics, soil structures were categorized as humic, poor, normal, or good (Table 1).

Table 1. Soil structure classes according to the ESDAC classification.

Soil Structure Class	ESDAC Classification
1—very fine granulation	Good
2—fine granulation	Normal
3—medium or coarse granulation	Poor
4—blocky, plastic, or massive structure	Humic

3.2.5. Soil Permeability (p)

Soil permeability classes were assigned based on the soil texture classes described in USDA, 1983 [62] (Table 2).

Table 2. Soil permeability classes based on soil texture.

Soil Permeability Class	Texture
1—rapid	Sand
2—moderate or rapid	Loamy sand, sandy loam
3—moderate	Loam, silty loam, silt
4—slow or moderate	Sandy clay loam, clay loam
5—slow	Silty clay loam, sandy clay
6—very slow	Silty clay, clay

3.3. Development of the RUSLE Model Factors for Soil Erosion Estimation

The RUSLE is an empirical model used to estimate soil erosion. The equation (Equation (1)) calculates the average annual soil loss (A) as follows:

$$A = R \times K \times LS \times C \times P \quad (1)$$

where A is average annual soil loss rate (t ha^{-1} $year^{-1}$); R is rainfall erosivity factor (MJ mm ha^{-1} h^{-1} $year^{-1}$); K is soil erodibility factor (t ha h ha^{-1} MJ^{-1} mm^{-1}); LS is topographic factor (dimensionless); C is a cover management factor (dimensionless); and P is a support practice factor (dimensionless).

3.3.1. Rainfall Erosivity Factor (R)

The R factor in the USLE and RUSLE models represents rainfall erosivity. In the original USLE framework, rainfall erosivity is defined based on storm kinetic energy and maximum 30-min rainfall intensity (EI_{30}) derived from standard plot conditions, where other RUSLE factors are assumed constant. This factor measures the impact of rainfall on soil erosion, a relationship initially observed through sediment deposits after

intense storms [30]. The R factor reflects the erosive force of rainfall, quantifying the kinetic energy of raindrops and the potential for resulting runoff in terms of volume and rate [31,63]. Calculating the R factor can be challenging because comprehensive rainfall data may not be available in all regions. Accurate localized precipitation data are essential for precisely computing the R factor, underscoring the link between rainfall characteristics and soil erosion potential. The study uses the MeteoSerbia1km dataset, the first daily gridded meteorological dataset at a 1 km spatial resolution across Serbia for the 2000–2019 period [64].

The empirical equation (Equation (2)), originally developed by Arnoldus (1977) [65] for estimating rainfall erosivity, and later corrected to properly incorporate the conversion factor [66] (Chen et al., 2023), was used due to the lack of high-temporal-resolution rainfall intensity data for the study area as follows:

$$R = 17.02 \times 10^{(1.5 \times \log\log \sum_{1}^{12} \frac{P_i^2}{P} - 0.8188)} \quad (2)$$

where R—rainfall erosivity factor in MJ mm ha^{-1} h^{-1} year^{-1}, P_i—monthly precipitation in mm, and P—annual precipitation in mm.

The ArcMap 10.4.1 Model Builder was employed to automate the processing of raster-based precipitation data. The process started with data normalization, as all original datasets are stored as integers (INT32 data type) to reduce the size of the GeoTIFF files. Precipitation rasters are divided by 10 to obtain precipitation data in millimeters.

After normalizing the data, the annual R factor was computed using the Raster Calculator tool. To obtain a long-term perspective on rainfall erosivity, the annual R factors were averaged over the 18-year study period using the Cell Statistics tool (data from the 2000 were excluded due to missing monthly datasets in the Zenodo repository).

3.3.2. Soil Erodibility Factor (K)

The Soil Erodibility Factor (K) quantifies the resistance of soil or surface materials to erosion by evaluating their susceptibility to detachment and transport by rainfall and runoff. K factor assesses the soil's ability to withstand the impact of raindrops and the consequent rate and volume of runoff under standardized conditions [67]. The K factor is derived using Equation (3) [30,31]:

$$K = \frac{2.1 \times 10^{-4} M^{1.14} (12 - OM) + 3.25(s - 2) + 2.5(p - 3)}{100} \times 0.1317 \quad (3)$$

where K—soil erodibility factor (t ha h ha^{-1} MJ^{-1} mm^{-1}), M—particle size parameter, calculated as (% silt + % very fine sand) × (100 − % clay), OM—organic matter (%), calculated by multiplying TOC by the Van Bemmelen factor (1.724), s—soil structure code, p—soil permeability class, 0.1317—factor for conversion to SI units. Due to the limited number and spatial distribution of soil samples (n = 46), the K factor was interpolated using the Inverse Distance Weighting (IDW) method and interpreted as a generalized spatial representation.

3.3.3. Slope Length and Slope Steepness Factor (LS)

The topographic factor (LS) is the soil loss ratio at a specific site compared to a baseline site, with a standard slope steepness of 9% and a slope length of 22.13 m [68]. LS factor includes two primary components: the slope length factor (L) and the slope steepness factor (S) [69]. Each component contributes to the rate of soil erosion on a given landscape. As the slope length increases, more runoff accumulates and flows downhill, increasing soil

erosion. Similarly, increased slope steepness causes runoff to move faster, enhancing its ability to erode soil [63,70].

To calculate the LS factor, data from the Shuttle Radar Topography Mission (SRTM) [71], a digital elevation model (DEM) with a 30 m × 30 m resolution, were used. This is the highest-resolution topographic dataset currently available for Serbia. A detailed assessment of the topographic conditions contributing to soil erosion was provided using these high-resolution data. The DEM was preprocessed by applying a fill-sinks algorithm developed by Wang and Liu (2006) [72], which effectively identifies and removes surface depressions in the elevation data. The methodology for calculating the LS factor was based on the approach proposed by Moore et al. (1991) [73], which integrates both slope length and slope steepness.

3.3.4. Cover Management Factor (C)

The cover management factor (C) reflects how different land cover types affect soil protection against erosion. Vegetation cover acts as a barrier shielding the soil surface from the direct impact of raindrops and dissipating their energy of the raindrops [74] before they reach the soil. Vegetative characteristics influence the soil's ability to absorb water, slow down runoff, and thus reduce the potential for erosion. The value of the C factor is directly influenced by vegetation type, growth stage, and the percentage of the ground covered by vegetation [67].

The C factor values are assigned to all land use types based on the values cited in the literature [44,75]. The ESA WorldCover dataset, based on Sentinel-1 and Sentinel-2 data, was used as the land cover input [76]. The ESA WorldCover data, initially at 10 m × 10 m resolution, was resampled to 30 m × 30 m using nearest-neighbor interpolation to align with other datasets and ensure consistency in the analysis. The C factor values assigned to specific land cover types ranged from 0 for built-up areas, permanent water bodies, and herbaceous wetlands, where soil erosion is effectively absent due to sealed or non-erodible surfaces, to 0.004 for tree cover, 0.05 for shrubland, 0.1 for grassland, 0.15 for cropland, and 0.3 for bare or sparsely vegetated areas.

3.3.5. Support Practice Factor (P)

The support practice factor (P) value is the ratio of the amount of soil loss after soil conservation measures to the amount of soil loss without any soil conservation measures [77,78]. Field observations revealed that no specific soil conservation practices, such as contour farming, strip cropping, terracing, grassed waterways, windbreaks or conservation tillage, are currently in place in the study area. Therefore, the P factor has been set to 1.0 throughout the entire region, meaning that no interventions to reduce soil loss from erosion are considered in the erosion estimates, and the current erosion susceptibility of the terrain is fully represented. Similar assumptions have been made in previous studies, where the P factor was also set to 1.0 in the absence of soil conservation practices [79–84].

3.4. Statistical Analysis

Statistical analysis was performed for each input factor of the RUSLE model and for the resulting erosion rates, including minimum, maximum, range, mean, standard deviation, coefficient of variation, and percentiles (5th, 25th, 50th [median], 75th, and 95th). For that purpose, raster layers generated in the GIS environment were used, including those for rainfall erosivity (R), soil erodibility (K), slope length and steepness (LS), cover management (C), and erosion rates (t ha^{-1} $year^{-1}$). Data processing in QGIS 3.40.4 [85] included raster preparation, reprojection, resampling, map algebra, and spatial overlay operations. The K factor was derived from soil property data obtained at 46 sampling locations and interpolated to a continuous raster, while the LS factor was calculated from a

DEM, and the C factor was assigned based on land cover data. Statistical analysis of raster layers was performed in SAGA GIS 9.7.1 using the Spatial and Geostatistics—Statistics for Grid module [86].

Additionally, the relationships between the calculated RUSLE erosion rates and the individual RUSLE factors, as well as selected soil properties, were examined through Spearman correlation analysis (ρ). This non-parametric approach was chosen because the data deviated from normality, as indicated by the Shapiro–Wilk test [87]. Correlation coefficients and corresponding *p*-values were calculated to assess the strength and statistical significance of the relationships. Regression analysis was additionally performed to analyze the contribution of interactions between the RUSLE factors. Calculations were conducted using Excel software [88].

4. Results and Discussion

The results of this study are presented in terms of the RUSLE factors—rainfall erosivity (R), soil erodibility (K), slope length and steepness (LS), and cover management (C)—as well as the calculated soil erosion rates, with detailed values for each sampling location provided in Table A1. In addition, the USDA textural classification of the soil samples, colored according to EU erosion severity classes, is shown in Figure A1.

4.1. Analysis of Rainfall Erosivity (R) Factor

The rainfall erosivity factor in the study area ranges from 1194.9 to 3117.7 MJ mm ha^{-1} h^{-1} year^{-1}, with a mean value of 1586.3 (Table 3). The dataset shows a noticeable range of values (1922.8 MJ mm ha^{-1} h^{-1} year^{-1}) and a standard deviation of 341.8, suggesting some variability in rainfall patterns and their erosive potential across the catchment. However, the coefficient of variation (CV = 22%) indicates that this variability is moderate rather than high, implying a relatively consistent R factor values within the catchment. The R factor distribution shows a clear gradient, with higher values observed in the mountainous regions (Figure 2), particularly in the western part of the basin, where the highest values are recorded on Kopaonik, the highest mountain in the study area. This trend aligns with the overall decrease in annual precipitation from west to east across Serbia [89,90]. Elevated precipitation values are also observed in the northern and southern mountainous areas, such as Jastrebac and Radan, consistent with previous studies [91,92]. In contrast, the lowest R factor values are found in the lower-lying areas, particularly in the valleys of the Toplica River and its main tributaries, as well as in the eastern parts of the basin. The distribution of R factors likely reflects climatic variations in precipitation and topographical influences on rainfall patterns.

Table 3. Descriptive statistics of RUSLE erosion factors and RUSLE erosion rates in the study area.

RUSLE	Rainfall Erosivity (R) (MJ mm ha^{-1} h^{-1} year^{-1})	Soil Erodibility (K) (t ha h ha^{-1} MJ^{-1} mm^{-1})	Slope Length and Slope Steepness (LS)	Cover Management (C)	Erosion Rate (t ha^{-1} year^{-1})
Min	1194.9	0.0155	0.000	0.0000	0.00
Max	3117.7	0.0676	73.153	0.3000	397.09
Rng	1922.8	0.0521	73.153	0.3000	397.09
Avg	1586.3	0.0436	4.123	0.0397	5.45
SD	341.8	0.0073	3.334	0.0541	12.20
CV (%)	22	17	81	136	224
5th percentile	1274.1	0.0317	0.430	0.0041	0.78
25th percentile	1379.6	0.0387	1.578	0.0041	2.34
50th percentile (median)	1455.1	0.0440	3.586	0.0041	3.89
75th percentile	1651.1	0.0493	6.455	0.1006	8.57
95th percentile	2359.9	0.0538	10.471	0.1500	31.92

Legend: Min—Minimum value, Max—Maximum value, Rng—Range, Avg—Average value, SD—Standard deviation.

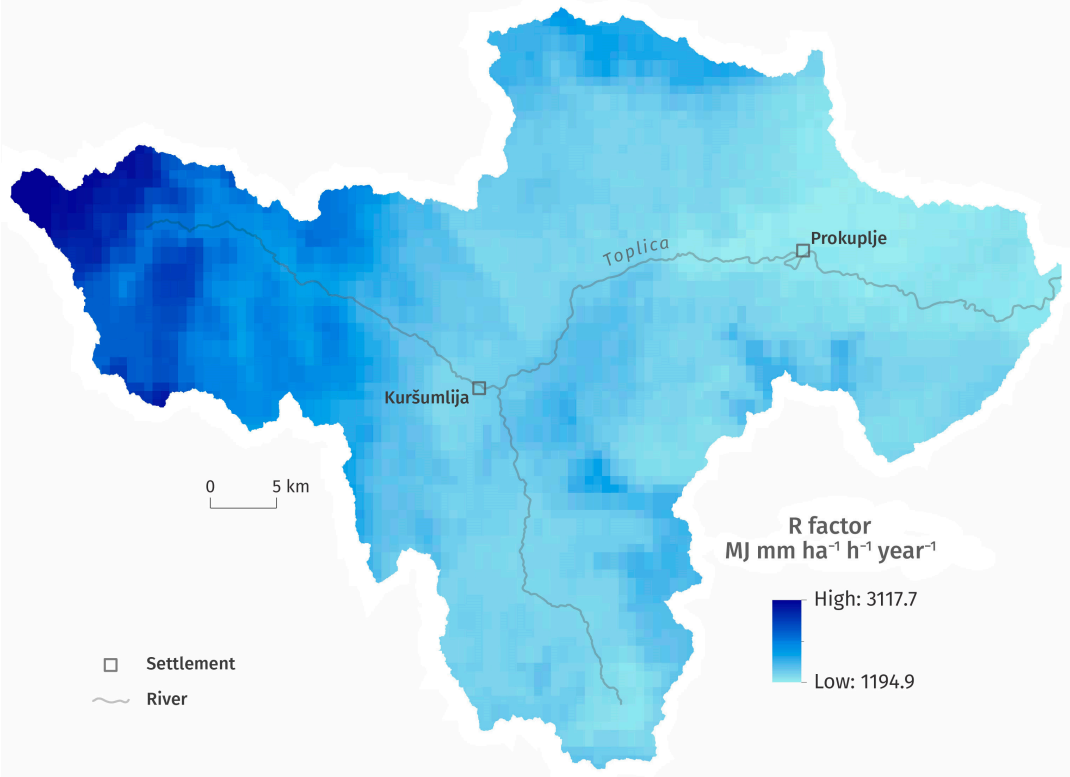


Figure 2. The R factor map of the study area for the period 2001–2019 (MJ mm ha^{-1} h^{-1} year^{-1}).

Both the mean value and the percentile distribution (Table 3) indicate that lower R factor values predominate. The fact that the 5th percentile (1274.1 MJ mm ha^{-1} h^{-1} year^{-1}) is relatively close to the mean (1586.3 MJ mm ha^{-1} h^{-1} year^{-1}), while the 95th percentile (2359.9 MJ mm ha^{-1} h^{-1} year^{-1}) is much higher, indicates a right-skewed distribution. Most areas within the basin experience moderate to low rainfall erosivity, while a few locations are subjected to intense erosive rainfall events.

For comparison, previous studies conducted in similar areas in the broader region (Bosnia and Herzegovina) have reported R factor values ranging from 2778.82 to 3656.34 MJ mm ha^{-1} h^{-1} year^{-1} in the Pale Municipality [93], from 1288.01 to 1431.02 MJ mm ha^{-1} h^{-1} year^{-1} in the northern part of the country [94], and from 826.7 to 4934.5 MJ mm ha^{-1} h^{-1} year^{-1} in the Republic of Srpska [49]. Additionally, a study conducted in Northwestern Crete, Greece, which shares comparable Mediterranean climatic influences, reported R factor values ranging from 348 to 3687 MJ mm ha^{-1} h^{-1} year^{-1} [95].

4.2. Spatial Distribution of Soil Erodibility (K) Factor

In the study area, the soil erodibility factor ranges from 0.0155 to 0.0676 t ha h ha^{-1} MJ^{-1} mm^{-1}, with a total span of 0.0521 t ha h ha^{-1} MJ^{-1} mm^{-1} (Table 3). The mean value is 0.0436 t ha h ha^{-1} MJ^{-1} mm^{-1}, and a standard deviation of 0.0073 t ha h ha^{-1} MJ^{-1} mm^{-1}, along with a coefficient of variation of 17%, indicates that most soils have relatively similar erodibility properties. Moreover, the differences between the values of the 5th and 25th, 25th and 50th, 50th and 75th, and 75th and 95th percentiles (Table 3) are similar, indicating a uniform distribution of the K factor across the river basin, with few extreme outliers and no significant skew toward unusually high or low values. The spatial distribution of the soil erodibility factor (Figure 3) does not exhibit a clear pattern. Both high and low values are found across a range of elevations, from higher mountainous regions to lower-lying areas, and occur in a variety of soil types, geological formations, and vegetation cover types. The lack of a clear spatial trend suggests that soil erodibility in the study area is influenced by an

interplay of multiple factors, including soil texture, organic content, and local topography, rather than being primarily dictated by any single environmental variable.

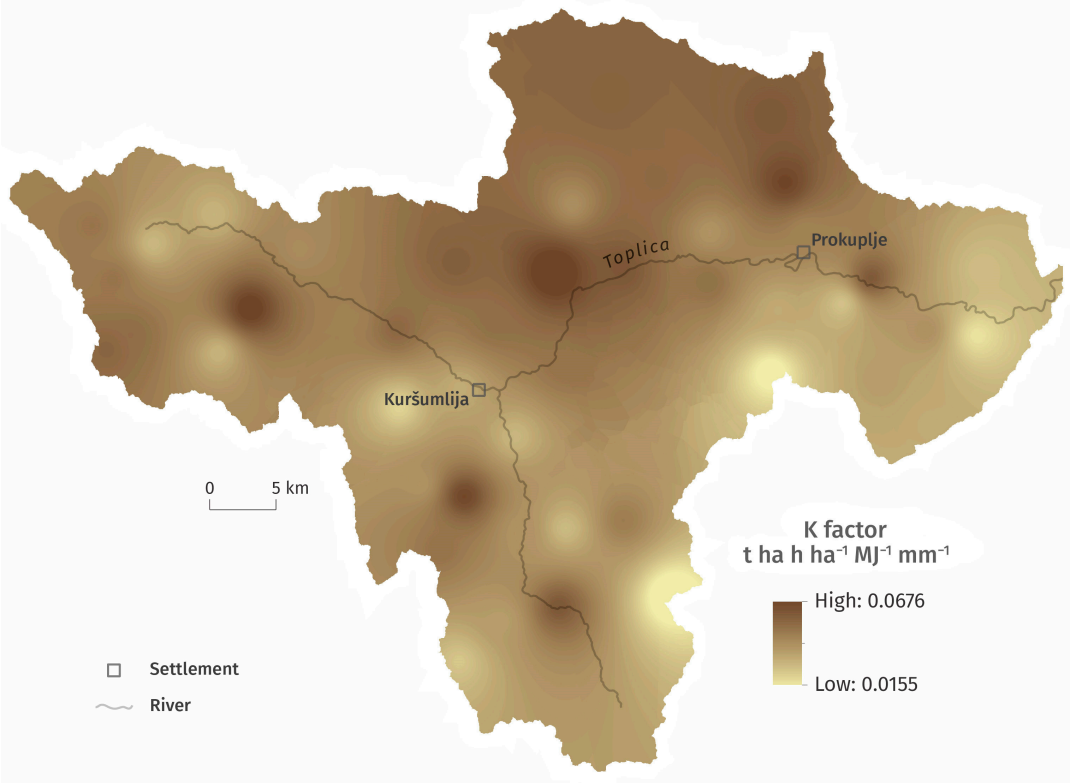


Figure 3. The K factor map of the study area (t ha h ha^{-1} MJ^{-1} mm^{-1}).

In line with this interplay of multiple controlling factors, the distribution of the K factor, which characterizes soil susceptibility to erosion, shows no clear spatial pattern and is influenced by individual sampling points. While this provides a general overview of areas with relatively higher or lower soil erodibility, local values may be over- or underestimated, particularly in sparsely sampled areas. Consequently, the K-factor map should be used to identify broad spatial tendencies rather than precise site-specific predictions.

Previous studies in geographically and climatically comparable regions have reported the soil erodibility factor (K) in the range of 0.01 to 0.08 t ha h ha^{-1} MJ^{-1} mm^{-1} in Romania [50], 0 to 0.07 t ha h ha^{-1} MJ^{-1} mm^{-1} in Southeastern Serbia [48] and Pirot Municipality, Serbia [46], and 0 to 0.061 t ha h ha^{-1} MJ^{-1} mm^{-1} in the Republic of Srpska (Bosnia and Herzegovina, BiH) [49]. These studies, conducted in areas with similar topographic and climatic conditions, show soil erodibility orders of magnitude similar to those observed in our study area, further supporting the consistency of soil erodibility characteristics across the region.

4.3. Analysis of Slope Length and Steepness (LS) Factor

The LS erosion factor ranges from 0 to 73.153, with an average of 4.123 and a standard deviation of 3.334 (Table 3; Figure 4). The highest LS values are found in the mountainous areas, particularly in the western part of the basin in Kopaonik, where the terrain is steep and dissected. Additionally, higher LS values are observed in the mountains to the north and south of the river basin, where steep slopes are common. It should be emphasized that the 30 m DEM resolution may smooth local slope extremes and underestimate absolute LS magnitudes in these steepest parts of the study area. On the other hand, lower LS values are recorded in the river valleys, particularly along the main river, Toplica, and in the flatter

terrain north of the Toplica River and the downstream, eastern part of the river basin. These areas, with gentler slopes and lower LS values, reflect the reduced potential for erosion.

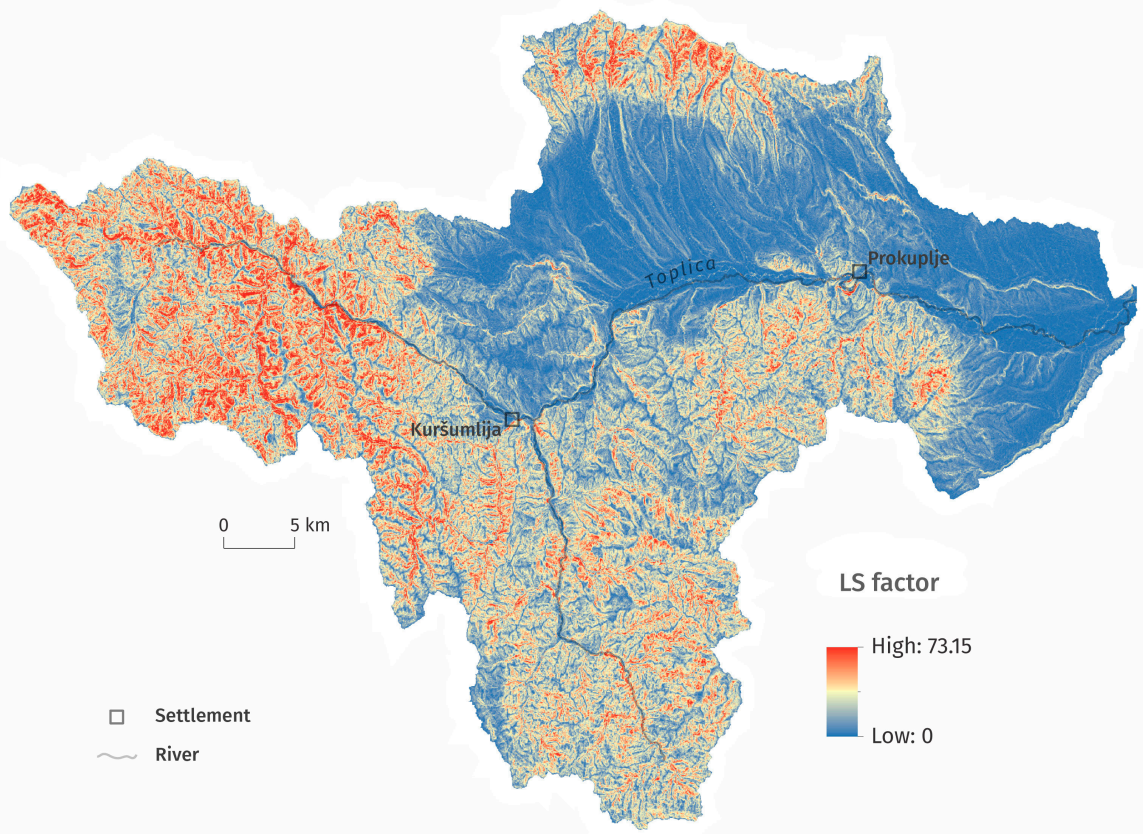


Figure 4. The LS factor map of the study area.

The differences between the 25th and 50th percentile values, as well as between the 50th and 75th percentile values, are nearly identical, indicating a relatively consistent distribution of LS values within these ranges (Table 3). However, the difference between the 5th and 25th percentile values is considerably smaller than between the 75th and 95th percentile values. This pattern suggests that higher LS values are less frequent. Additionally, the difference between the minimum value (0) and the 5th percentile is much smaller than that between the 95th percentile and the maximum value (73.153), further supporting the idea that extreme values are rare.

In the Pirot Municipality, Serbia, values of the LS factor reflected a similar distribution, with steep, dissected mountainous areas showing higher values [46]. Similarly, in the Lower Kulsi Basin, India, the LS factor ranged from 0 to 80.5 [96], showing a pattern of higher values in steeper terrain and lower values in flatter areas, which aligns with the findings of our study.

4.4. Cover Management (C) Factor Analysis

The distribution of land cover types within the basin, derived from ESA data (Table 4), plays a crucial role in determining the cover management factor (C) and its influence on erosion potential. Forested areas (tree cover) dominate the landscape, covering 67% of the basin, predominantly in the mountainous and hilly regions in the north, west, and south.

Table 4. Land cover types and their respective areas based on ESA data.

Land Cover ESA	Area (km^2)	Area (%)
Tree cover	1474.27	67.116
Shrubland	0.07	0.003
Grassland	471.58	21.469
Cropland	225.83	10.281
Build-up	24.03	1.094
Bare/Sparse vegetation	0.47	0.021
Permanent water bodies	0.26	0.012
Herbaceous wetland	0.08	0.004

Forested areas are interspersed with grassland, forming a mosaic-like pattern, except on Jastrebac Mountain, where continuous forested expanses prevail. Due to dense vegetation and well-developed root systems, tree-covered areas contribute to lower C values, offering significant protection against soil erosion by reducing raindrop impact, surface runoff, and soil detachment (Figure 5). Grassland, occupying 21% of the basin provides moderate erosion protection. Compared with forest cover, grassland exhibits slightly higher C values due to its lower canopy cover and weaker root structures, which allow increased surface runoff and soil displacement in steeper regions. Cropland, covering 10% of the basin, is predominantly located in the lower reaches of the Toplica River, in the eastern part of the basin, and in the valley between the Toplica River and the slopes of Jastrebac Mountain. These areas, particularly when cultivated with annual crops and subjected to tillage, exhibit the highest C values, making them more vulnerable to soil erosion. The lack of permanent vegetation cover increases exposure to rainfall impact and surface runoff, leading to increased soil loss.

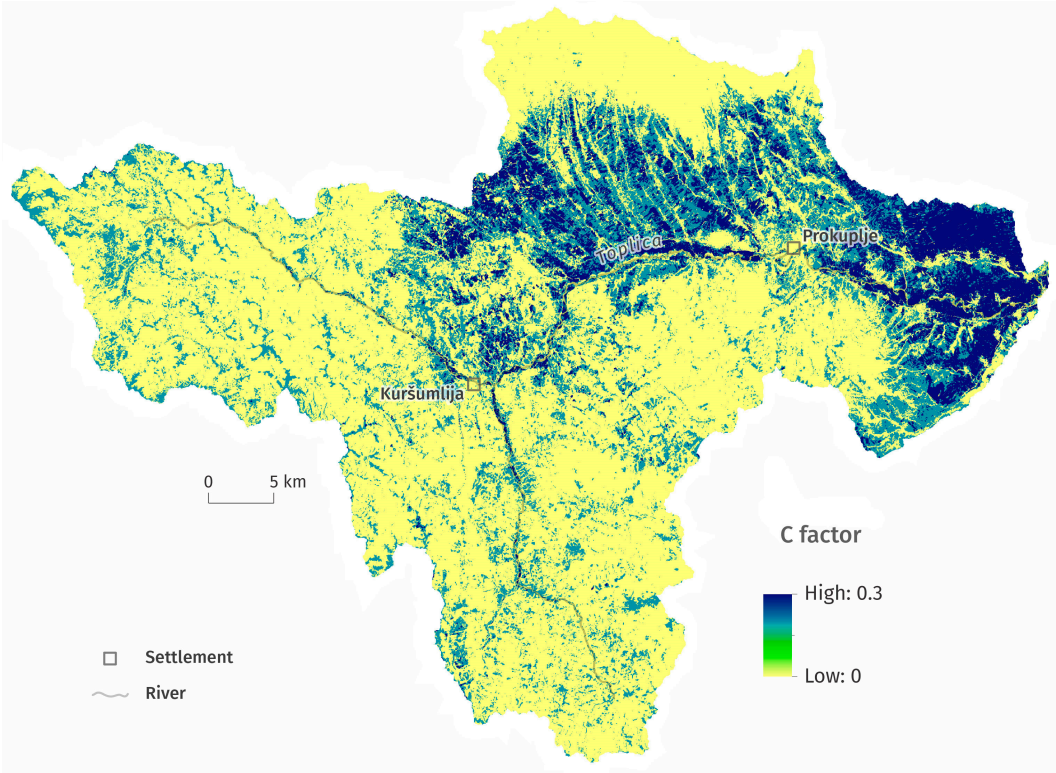


Figure 5. The C factor map of the study area.

Although occupying a smaller portion of the basin, built-up areas (1.094%) and bare or sparsely vegetated surfaces (0.021%) also contribute to variations in erosion susceptibility.

While built-up surfaces are largely impervious, preventing soil erosion directly, bare areas exhibit some of the highest C values due to minimal vegetation cover and increased susceptibility to surface runoff. Other minor land cover classes, including shrubland (0.003%), permanent water bodies (0.012%), and herbaceous wetlands (0.004%), have negligible effects on overall erosion processes. However, despite their small coverage, wetlands can act as sediment retention zones, helping reduce sediment transport in localized areas.

The types of land cover across the basin strongly influence the C factor. Forested areas tend to have the lowest erosion potential, while cropland and bare soil contribute more to erosion risks. This pattern clearly shows the importance of land cover in mitigating erosion, highlighting the need for sustainable land use and cover to minimize soil loss.

The descriptive statistics (Table 3) support this pattern, as over half of the basin has very low C values ($\leq$0.0041), which are mostly associated with forest and grassland. However, higher C values appear in the upper percentiles, for example, 0.1006 at the 75th percentile and 0.1500 at the 95th percentile, reflecting cropland and sparsely vegetated areas. While the maximum C value (0.3) indicates a potential for high erosion risk, such extreme values are rare, reinforcing that most of the basin is covered by areas less prone to erosion, such as forests and grasslands.

4.5. Soil Erosion Rates from RUSLE

The results of the RUSLE model exhibit substantial spatial heterogeneity across the study area, which can be attributed to the combined influence of multiple erosion factors with varying magnitudes and spatial distributions. Despite this complexity, several general patterns of estimated soil erosion intensity can be identified. Although some parts of the basin exhibit high erosion rates, most of the watershed falls onto the low-erosion category, with soil loss values below 5 t ha^{-1} year^{-1}. As shown in Table 5, low erosion areas (<5 t ha^{-1} year^{-1}) cover approximately 78% of the watershed, with the most considerable portion falling within the 2–5 t ha^{-1} year^{-1} range (24%) and the 1–2 t ha^{-1} year^{-1} range (26%). These classifications are based on the thresholds used by the European Union [97]. Moderate erosion rates (5–10 t ha^{-1} year^{-1}) cover 8% of the basin, while severe erosion areas (>10 t ha^{-1} year^{-1}) account for 13% of the total area, with only 1.5% experiencing rates exceeding 50 t ha^{-1} year^{-1}.

Table 5. Classification of soil erosion rates and area distribution in the study area based on RUSLE.

Erosion Class	Erosion Rate (t ha^{-1} year^{-1}) *	Area (km^2)	Area (%)
Low	<0.5	273.73	12.46
	0.5–1	365.01	16.62
	1–2	566.21	25.78
	2–5	524.58	23.88
Moderate	5–10	180.71	8.23
Severe	10–20	149.81	6.82
	20–50	103.42	4.71
	>50	33.11	1.51

* Soil erosion rate classes are defined as half-open intervals, where the lower boundary is inclusive and the upper boundary is exclusive.

The highest erosion rates are observed in the western part of the basin, particularly on the eastern slopes of Kopaonik (Figure 6). This pattern is likely influenced by the high rainfall erosivity in this area, combined with the significant slope length and steepness, which are among the highest in the basin. The C factor indicates that this area is mostly forested, with some grassland patches. While both types of vegetation help reduce erosion,

the protective effect is lower on steep slopes and in locations subject to intense rainfall, leading to locally elevated soil loss rates.

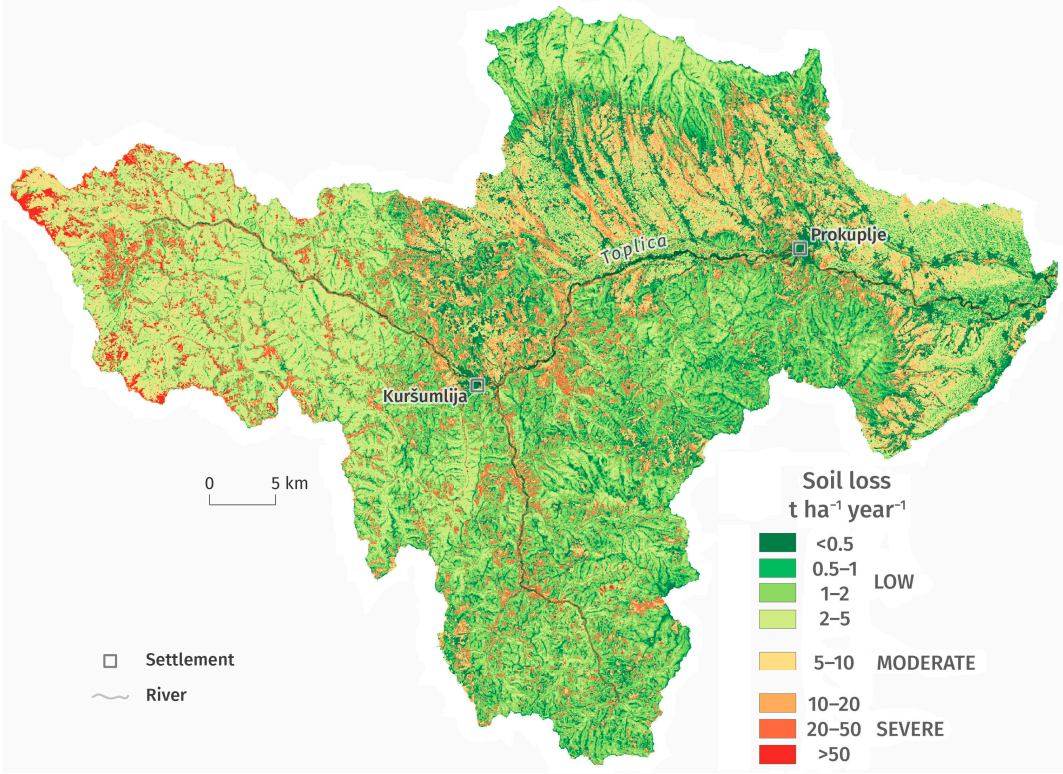


Figure 6. RUSLE distribution of different soil erosion classes for the study area.

Erosion is predominantly low intensity in the basin's southern part, despite the dominance of hilly and mountainous terrain. A mosaic of moderate-to-severe erosion patches is present in this region, likely due to variations in land cover and local slope conditions. The extensive forested areas in these southern mountainous regions play a crucial role in reducing the potential for erosion, as indicated by the low C factor values. In this region, R and K factors have moderate values and play a relatively minor role in controlling erosion compared to land cover and local slope variations. The lowest erosion rates are estimated in the northern part of the basin, particularly in the Jastrebac Mountain region, where nearly the entire mountain area falls into the low erosion category due to dense forest cover.

In lower-altitude areas with prevalent cropland, the highest erosion rates are observed in the basin's central part. This is likely due to the hilly terrain, with slope gradients that enhance soil loss and the lack of forest cover in this region. While the LS factor values in the central part are lower than those in the mountainous region, they remain significant due to terrain's hilly, moderately dissected nature. Although these areas lack the steep slopes characteristic of mountainous zones, the terrain is not entirely flat and still allows surface runoff. In combination with intensive land use, they contribute to substantial erosion. Although the absolute highest erosion values are recorded in the steep western slopes of the basin, the combined effects of terrain, land use, and vegetation cover suggest that, on average, erosion in the central part is among the most pronounced.

In areas with moderate to severe erosion risk, appropriate soil conservation measures are essential to prevent further degradation. Practical strategies commonly used include conservation tillage, cover crops, contour farming, mulching, and terracing, which have been shown to significantly reduce soil loss by increasing soil surface cover, improving infiltration, and reducing runoff impacts. The effectiveness of these practices depends on local conditions, but overall they can reduce current erosion of agricultural and semi-natural

landscapes [98–102]. In the cropland areas downstream of the Kosanica River confluence (Figure 1), elevated erosion rates occur despite moderate slope gradients and reduced rainfall erosivity. This suggests that current land use practices significantly determine soil loss, and without mitigation measures, erosion rates could rise rapidly, under increasing social and environmental pressures. Based on a large-scale review of global data, Yang et al. (2023) [103] showed that vegetation restoration through forest and grassland cover significantly reduces runoff and soil erosion while enhancing soil carbon and nitrogen content, particularly in the upper soil layers. Similarly, Thiengo et al. (2024) [104] found that conventional tillage practices on steep slopes lead to substantially greater soil and water losses, whereas no-tillage systems, especially when integrated with tree cover, effectively minimize erosion and improve soil conservation. These findings align with the national-scale study by Feeney et al. (2023) [105] in Kenya, which reported that erosion rates on cropland are nearly three times higher than those under natural vegetation, resulting in widespread topsoil depletion and a reduced soil lifespan.

The lowest erosion values (<0.5 t ha^{-1} year^{-1}) are primarily found in built-up areas, including two cities and several villages, and are generally located on gentle slopes in areas with low R factor values. Urban and infrastructural areas are typically partially covered by impervious surfaces, such as asphalt and concrete, for which a C factor of 0 is applied in the RUSLE model, resulting in effectively zero erosion rates, regardless of other erosion factors. Overall, the spatial patterns of erosion intensity in the watershed align well with the distribution of the RUSLE factors, reinforcing the importance of integrating multiple erosion drivers when assessing soil loss potential. These results provide a solid foundation for future land management and conservation strategies to mitigate soil erosion in vulnerable areas.

The statistical data (Tables 3 and 5) confirm the dominance of low-erosion areas within the RUSLE framework. The mean erosion value across the area is 5.45 t ha^{-1} year^{-1}, indicating a relatively moderate average level of erosion. However, there is a wide range of erosion values, with a minimum of 0 t ha^{-1} year^{-1} and a maximum of 397.09 t ha^{-1} year^{-1}. The standard deviation of 12.20 t ha^{-1} year^{-1}, along with a high coefficient of variation (CV = 224%), suggests considerable variability in erosion rates across the basin. The occurrence of extreme erosion values in the study area is strongly influenced by the LS factor, as highlighted in previous studies [47]. Among all RUSLE factors, the LS factor generally influences extreme erosion values, contributing to localized high erosion estimates. This aligns with findings that the RUSLE model, due to its sensitivity to topographic conditions, can overestimate erosion in areas with highly complex slopes [106]. The highest extreme values are predominantly found on Kopaonik Mountain, where steep slopes coincide with sparse vegetation cover. Notably, these extreme erosion rates do not occur in forested areas but are primarily found in grassland regions, where soil exposure is more significant. This area also exhibits the highest rainfall erosivity (R factor) values in the basin, further amplifying erosion potential. However, the occurrence of such extreme erosion values exceeding 100 t ha^{-1} year^{-1} remains very rare. These values appear as isolated pixels or small pixel groups on the erosion map, where all major erosion factors coincide at their highest values. This spatial distribution underscores the localized nature of extreme erosion estimates and highlights the necessity for careful interpretation when assessing model outputs.

The Spearman correlation analysis indicates varying degrees of association between erosion rates and the individual contributing factors (K, R, LS, and C) (Table 6). The highest correlation was observed with the C factor ($\rho = 0.568$, $p < 0.01$), followed by the LS factor ($\rho = 0.461$, $p < 0.01$) and the R factor ($\rho = 0.301$, $p < 0.05$), indicating different degrees of impact on erosion rates. This suggests that land cover (C factor) is the most influential determinant of soil erosion intensity, followed by topographic characteristics

and rainfall erosivity. In contrast, the negative correlation with the K factor was very weak and statistically non-significant (ρ = −0.032, p = 0.835), reflecting the relatively uniform distribution of K factor values across the river basin. This highlights the complexity of erosion processes and the need for integrated assessments that account for interactions among different environmental variables.

Table 6. Spearman correlation coefficients and corresponding p-values between erosion rates, elevation, selected soil properties, and RUSLE input factors at sampling locations.

	Variable	ρ	p-Value
Soil properties	Elevation	0.159	0.291
	BD	0.138	0.359
	TOC	0.089	0.556
	Clay	0.192	0.201
	Silt	0.335 *	0.023
	Fine sand	−0.376 **	0.01
	Coarse sand	−0.154	0.307
	Skeleton	0.105	0.489
RUSLE factors	K	−0.032	0.835
	R	0.301 *	0.042
	LS	0.461 **	0.001
	C	0.568 **	0

* Correlation is significant at the 0.05 level. ** Correlation is significant at the 0.01 level.

The correlation coefficients between erosion rates at sampling locations and soil properties (total bulk density, organic carbon, clay, silt, fine sand, coarse sand, and skeletal content) indicate mostly weak relationships (Table 6). The strongest correlations were observed with fine sand and silt contents, showing a statistically significant moderate negative correlation for fine sand (ρ = −0.376, $p < 0.01$) and a statistically significant moderate positive correlation for silt (ρ = 0.335, $p < 0.05$). Clay content showed a slight positive correlation that was not statistically significant (ρ = 0.192, p = 0.201), while coarse sand demonstrated a weak negative and non-significant correlation (ρ = −0.154, p = 0.307). Bulk density (ρ = 0.138, p = 0.359), skeleton content (ρ = 0.105, p = 0.489), and TOC (ρ = 0.089, p = 0.556) showed negligible, statistically non-significant correlations, indicating minimal influence on erosion rates. Although the direct correlations between soil properties and erosion rates are generally weak, their role remains important through their contribution to the soil erodibility factor (K), underscoring the need to consider soil properties within the broader context of interacting environmental factors. The erosion rate shows no significant linear correlation with elevation (ρ = 0.159, p = 0.291). Differences in erosion rates across elevation classes were also not significant, and the pronounced intra-class variability demonstrates the combined effects of local factors within each elevation zone (Appendix C). Consequently, elevation influences erosion primarily through its association with topography, climate, and land-use patterns in the study area. Overall, correlation analysis suggests that soil erosion in the study area is not driven by individual soil properties or elevation but rather by complex interactions within the catchment.

In addition to linear correlation, regression analysis was used to examine the influence of individual factors and their interactions on the spatial variability of predicted erosion rates (Table 7). The RUSLE factors were standardized prior to the analysis to reduce scale-related bias and enable direct comparison of their contributions. Using only RUSLE factors, the linear regression model confirmed the dominant role of the C factor with the highest standardized regression coefficients (β = 0.508), followed by the R and LS factors (β = 0.382 and β = 0.338, respectively), while the influence of factor K was not significant (β = 0.128) in controlling predicted soil loss. However, this model explained only 52% of the variance

(R^2 = 52.45%, R^2adj = 47.81%) and showed limited predictive capability (R^2pred = 24.82%, Bayesian Information Criterion, BIC = 118.31), with a relatively high standard error of regression (S = 0.723).

Table 7. Regression analysis of RUSLE-predicted erosion rates (Predictor = RUSLE factor, quadratic term, or interaction; β = standardized regression coefficient; SE β = standard error of β; *p*-Value = test statistic for significance; VIF = variance inflation factor; S = standard error of the model; R^2, R^2adj, R^2pred = explained, adjusted, and predicted variance (%); BIC = Bayesian Information Criterion).

Regression Model	Predictor	β	SE β	*p*-Value	VIF	S	R^2 (%)	R^2adj (%)	R^2pred (%)	BIC
Linear regression model	Constant	−0.000	0.107	1.000		0.723	52.45	47.81	24.82	118.31
	K	0.128	0.108	0.241	1.00					
	R	0.382	0.122	0.003	1.28					
	LS	0.338	0.129	0.012	1.42					
	C	0.508	0.115	0.000	1.14					
Multiple linear regression model including quadratic terms and pairwise interactions	Constant	0.093	0.049	0.068		0.125	98.93	98.44	92.55	−17.87
	K	0.253	0.023	0.000	1.50					
	R	0.080	0.052	0.136	7.85					
	LS	0.828	0.035	0.000	3.47					
	C	0.731	0.025	0.000	1.80					
	K^2	0.044	0.022	0.056	2.24					
	R^2	−0.005	0.029	0.855	7.79					
	LS^2	−0.079	0.023	0.002	9.24					
	C^2	0.022	0.040	0.579	2.14					
	K × R	0.106	0.030	0.001	1.53					
	K × LS	0.231	0.036	0.000	2.04					
	K × C	0.120	0.020	0.000	1.27					
	R × LS	0.261	0.038	0.000	4.64					
	R × C	0.268	0.035	0.000	2.98					
	LS × C	0.561	0.050	0.000	7.89					

When quadratic and interaction terms were included to account for non-linear and combined effects between climatic, topographic, soil, and land-cover controls, the model performance dramatically improved, yielding R^2 = 98.93%, R^2adj = 98.44%, and R^2pred = 92.55%, with a substantial reduction in BIC (−17.87), and S (0.125) indicating strong internal consistency and predictive ability. The hierarchy of influence of the main factors on the normalized erosion rate also changed, indicating significant effects of LS (β = 0.828), C (β = 0.731), and K (β = 0.252), whereas the influence of R as a standalone factor was insignificant (β = 0.080). The most important finding of this analysis is the critical role of factor interactions (all interaction terms were statistically significant at $p < 0.01$), which accounted for most of the variance not explained by the linear model.

Among the interactions, LS × C had the strongest effect (β = 0.561), highlighting that vegetation's ability to reduce erosion is substantially limited on steeper slopes. Rainfall-related interactions, R × C (β = 0.268) and R × LS (β = 0.261), were next in importance, indicating that rainfall erosivity becomes a potent erosive force primarily when combined with steep slopes or poorly protected soils. Interactions involving soil erodibility (K × LS, K × C, K × R) had smaller but still significant effects, showing that the influence of K is amplified under less favorable conditions of the other factors. Finally, the limited importance of quadratic terms (except LS^2 with β = −0.079, $p < 0.002$) indicates that non-linearities are primarily expressed through interactions among factors rather than through isolated second-order effects of individual predictors.

It should be emphasized that the results and interpretations presented in this section are subject to the inherent and well-documented limitations of the RUSLE method. These limitations should be carefully considered when evaluating the findings, particularly with respect to data availability and the representation of individual erosion factors.

The K-factor map, representing soil erodibility, is based on a limited number of point samples that were interpolated to produce a continuous spatial representation. While efforts were made to select locations that best represent the study area, this interpolation inevitably introduces uncertainty. Local values may be over- or underestimated, and individual sampling points can exert a strong influence on the results, particularly in sparsely sampled areas. Consequently, the K-factor map provides reliable indications of general spatial tendencies across the study area, highlighting zones of relatively higher or lower soil erodibility, but may not fully capture fine-scale local variability. Therefore, the map is suitable for identifying broad patterns of erosion susceptibility, while detailed, site-specific interpretations should be treated with caution. Regarding the R factor, it should be noted that the applied values represent rainfall erosivity only. Snow cover and snowmelt processes are not explicitly accounted for. This may be relevant in mountainous areas where snow persists for a substantial part of the year. As a result, seasonal variations in erosivity, particularly those associated with spring snowmelt, may not be fully reflected in the modeled R-factor values.

Model validation represents another important source of uncertainty in RUSLE-based studies, as it is essential for assessing the reliability of modeled erosion patterns. External validation against field-measured erosion rates in the study area is not available, and no such measurements have been conducted to date, although they would be ideal for rigorous verification. To partially address this limitation, the modeled results were compared with findings from nearby or environmentally similar study areas, where comparable erosion patterns and magnitudes have been reported. The average annual soil loss in the present study (5.45 t ha^{-1} yr^{-1}) is of the same order of magnitude as values reported by Tošić et al. [49] for the Republic of Srpska (5.13 t ha^{-1} yr^{-1}) and Patriche [50] for Romania under current climate conditions (2.94 t ha^{-1} yr^{-1}). It remains considerably lower than the average erosion rate reported by Životić et al. [48] for the Nišava River basin (13.1 t ha^{-1} yr^{-1}), an area characterized by more pronounced erosion-prone conditions. Furthermore, the erosion rates in the present study span a wide range. Low to moderate values prevail over most of the area (median 3.89 t ha^{-1} yr^{-1}), while higher erosion rates occur locally. Given the similarities in applied methodology and environmental conditions, the consistency of erosion rates supports the reliability of the obtained results.

Beyond this comparative assessment, the predictive uncertainty of the modeled erosion rates was quantified using the regression framework (Table 7). For the best-performing model, the standard error of regression (S = 0.125, R^2pred = 92.55%) corresponds to an average absolute error of approximately ±2.2 t ha^{-1} $year^{-1}$ when expressed in physical units, representing about 18% of the mean erosion rate. While this approach does not replace external validation, it provides a quantitative measure of the internal uncertainty of the modeled erosion estimates at the sampling locations, demonstrates that the model captures the dominant controls and interactions governing spatial variability in erosion, and provides evidence of consistency with the physical processes.

In support of the obtained results, qualitative field observations conducted during sampling (e.g., occurrence of bare soil patches and slope instability) were consistent with areas identified by the model as having elevated erosion risk. Satellite imagery was also examined, particularly in mountainous areas such as the exposed surfaces of Kopaonik Mountain, further supporting the modeled erosion distribution.

5. Conclusions

This study applied an advanced GIS-based RUSLE framework, supported by field-derived soil data, to assess spatial patterns of soil erosion in the Toplica River Basin. The results confirm pronounced spatial variability in erosion intensity and demonstrate that

soil erosion is governed by the combined and interacting effects of topography, land cover, rainfall erosivity, and soil properties, rather than by any single dominant factor. Two prevailing erosion regimes were identified across the basin: topography-controlled erosion in mountainous areas and land-use-controlled erosion in low- to moderately sloping agricultural areas.

Although erosion rates are generally low across most of the study area, localized severe erosion zone hotspots (>10 t ha^{-1} $year^{-1}$) were identified. This is evident in the mountainous regions of Kopaonik, where intense erosion occurs in specific, smaller areas. However, since forests cover most of this terrain, they significantly mitigate susceptibility to soil loss. In contrast, in the flatter terrains of the central and eastern parts of the watershed, erosion remains significant despite the relatively low R factor and moderate LS values. This is primarily due to agricultural land use, where soil disturbance, reduced vegetation cover, and farming practices increase erosion rates.

The findings emphasize the need for spatially tailored soil conservation measures according to identified erosion regimes. Vegetation protection and slope stabilization are critical in mountainous erosion hotspots, whereas land-use-oriented practices are essential in agricultural hotspots, where erosion is primarily driven by soil disturbance rather than extreme terrain conditions. Although high-altitude areas are not always prioritized economically, erosion in these regions contributes to torrential flows, increased sediment transport, and downstream water pollution, necessitating targeted mitigation strategies. In fertile, low-erosion downstream areas essential for agriculture, preventive measures remain crucial to preserve soil productivity and long-term land sustainability. In these lowland regions, practices such as crop rotation, conservation tillage, contour farming, and the establishment of buffer strips along waterways can be particularly effective. Providing farmers with education on sustainable practices is essential to ensure the successful implementation of these measures and to promote long-term resilience of agricultural systems. These indicative recommendations should be interpreted with consideration of the uncertainties inherent to RUSLE application, particularly those related to the representation of K-factor and the validation constraints of the integrated approach.

Combining RUSLE modeling, soil characterization, and GIS-based spatial analysis provides a basis for identifying priority areas in the Toplica River and supporting region-specific erosion management.

Author Contributions: Conceptualization, M.Đ. (Milan Đorđević), M.Đ. (Mrđan Đokić), M.M., J.V., R.D., I.S., S.D. and A.O.; methodology, M.Đ. (Milan Đorđević), M.Đ. (Mrđan Đokić), M.M., J.V., R.D., I.S., S.D. and A.O.; software, M.M.; validation, M.Đ. (Milan Đorđević), J.V., I.S., S.D. and A.O.; formal analysis, M.Đ. (Milan Đorđević) and M.M.; investigation, M.Đ. (Milan Đorđević), M.M., J.V., R.D., I.S., S.D. and A.O.; resources, M.Đ. (Milan Đorđević); writing—original draft, M.Đ. (Milan Đorđević), M.Đ. (Mrđan Đokić), M.M., R.D., I.S. and S.D.; writing—review and editing, M.Đ. (Milan Đorđević), M.Đ. (Mrđan Đokić), M.M., J.V., R.D., I.S., S.D. and A.O.; visualization, M.Đ. (Milan Đorđević) and M.M.; supervision, M.Đ. (Milan Đorđević), R.D., I.S., S.D. and A.O.; project administration, S.D.; funding acquisition, M.Đ. (Milan Đorđević), M.Đ. (Mrđan Đokić), M.M., J.V., R.D., I.S., S.D. and A.O. All authors have read and agreed to the published version of the manuscript.

Funding: This research was supported by the Science Fund of the Republic of Serbia (grant No. 7047), Development of erosion prediction tool for sustainable soil management—Predict-Er. This paper was also supported by the Ministry of Science, Technological Development and Innovation of the Republic of Serbia (contracts 451-03-33/2026-03/200017, 451-03-34/2026-03/200124, and 451-03-137/2025-03/200116).

Data Availability Statement: The raw data supporting the conclusions of this article will be made available by the authors on request.

Conflicts of Interest: The authors declare no conflicts of interest. The funders had no role in the design of the study; in the collection, analyses, or interpretation of data; in the writing of the manuscript; or in the decision to publish the results.

Abbreviations

The following abbreviations are used in this manuscript:

CV	Coefficient of Variation
DB	Dry Bulk Density
DEM	Digital Elevation Model
EEA	European Environment Agency
ESA	European Space Agency
FAO	Food and Agriculture Organization
GIS	Geographic Information System
GPS	Global Positioning System
JRC	Joint Research Centre
OM	Organic Matter
RUSLE	Revised Universal Soil Loss Equation
SD	Standard Deviation
SRTM	Shuttle Radar Topography Mission
TOC	Total Organic Carbon
USDA	United States Department of Agriculture
USLE	Universal Soil Loss Equation

Appendix A

Table A1. Coordinates of sampling locations with information on corresponding altitude, soil properties, erosion factors, and erosion rates.

Sampling Location				Soil Properties							RUSLE Factors and Erosion Values				
Sampling Location Number	Latitude (°)	Longitude (°)	Altitude (m)	Bulk Density (g/cm^3)	TOC (%)	Clay (%)	Silt (%)	Fine Sand (%)	Coarse Sand (%)	Skeleton (%)	K Factor (t ha h ha^{-1} MJ^{-1} mm^{-1})	R Factor (MJ mm ha^{-1} h^{-1} year^{-1})	LS Factor	C Factor	Erosion Rate (t ha^{-1} year^{-1})
1	43.25428	20.89881	1018	0.99	1.08	21.7	43.7	11.5	23.1	36.8	0.0477	2609.27	5.63	0.004	2.80
2	43.16702	20.91309	1142	1.22	0.97	28.3	56.5	5.6	9.6	27.5	0.0521	2268.86	7.56	0.100	89.34
3	43.21659	20.91871	881	1.05	1.78	25.2	57.7	7.0	10.1	28.6	0.0478	2182.37	4.33	0.100	45.12
4	43.1772	20.9363	1033	1.16	1.48	21.7	55.2	6.6	16.5	35.2	0.0500	2298.55	1.34	0.100	15.43
5	43.24173	20.95783	894	0.95	2.40	19.0	34.9	8.8	37.2	33.7	0.0327	2277.56	5.28	0.100	39.36
6	43.26228	21.01607	880	1.02	4.18	14.5	55.7	10.2	19.6	23.3	0.0336	2019.80	3.55	0.100	24.11
7	43.16437	21.02054	734	1.18	2.91	9.9	34.9	15.3	40.0	48.3	0.0337	1976.44	6.56	0.100	43.60
8	43.19595	21.05118	939	1.07	2.85	13.5	60.7	7.1	18.6	23.7	0.0637	1958.73	3.12	0.100	38.96
9	43.23772	21.09967	797	1.5	1.20	18.9	40.1	8.1	33.0	43.4	0.0427	2016.46	14.87	0.004	5.12
10	43.18995	21.14969	585	1	2.95	10.4	48.9	15.1	25.5	42.6	0.0454	1751.18	6.57	0.004	2.09
11	43.12588	21.19559	539	1.2	4.68	15.1	36.4	22.5	26.1	37.5	0.0265	1541.88	4.16	0.004	0.68
12	43.18128	21.19328	431	1.4	1.22	16.3	34.8	22.1	26.8	30.8	0.0512	1533.12	3.83	0.100	30.11
13	43.07122	21.21556	493	1	0.93	14.7	32.7	13.1	39.5	32.7	0.0410	1492.27	8.37	0.004	2.05
14	43.02483	21.23519	710	1.3	1.60	12.2	41.8	12.3	33.7	40.7	0.0483	1530.57	8.87	0.004	2.62
15	42.94559	21.25266	565	1.3	4.62	18.2	47.6	21.2	13.0	40.0	0.0296	1394.83	1.32	0.100	5.44
16	43.22799	21.25035	415	1	0.82	28.4	46.7	15.3	9.6	68.6	0.0540	1552.74	0.24	0.150	2.99
17	43.13875	21.25452	437	1	1.42	23.0	28.2	13.8	35.1	52.1	0.0350	1392.47	2.43	0.100	11.87
18	43.06251	21.25815	428	1.2	2.35	9.9	42.6	33.5	14.1	20.2	0.0605	1427.96	1.35	0.004	0.47
19	43.18766	21.28861	528	1.08	0.52	31.1	38.5	17.8	12.6	54.8	0.0497	1481.28	0.36	0.100	2.64
20	42.97422	21.29293	462	1.37	1.43	25.2	25.4	18.2	31.3	52.7	0.0385	1429.65	3.43	0.100	18.91
21	43.03639	21.31422	421	1.01	0.90	23.2	31.8	14.6	30.3	53.8	0.0409	1370.06	4.59	0.100	25.75
22	43.10466	21.30749	401	0.94	3.70	16.7	48.4	9.1	25.9	34.9	0.0329	1532.71	3.05	0.100	15.42
23	43.22088	21.34605	311	1.11	0.45	10.6	24.2	42.3	22.9	29.6	0.0676	1365.34	0.19	0.004	0.07

Table A1. *Cont.*

Sampling Location				Soil Properties							RUSLE Factors and Erosion Values				
Sampling Location Number	Latitude (°)	Longitude (°)	Altitude (m)	Bulk Density (g/cm^3)	TOC (%)	Clay (%)	Silt (%)	Fine Sand (%)	Coarse Sand (%)	Skeleton (%)	K Factor (t ha h ha^{-1} MJ^{-1} mm^{-1})	R Factor (MJ mm ha^{-1} h^{-1} year^{-1})	LS Factor	C Factor	Erosion Rate (t ha^{-1} year^{-1})
24	42.98402	21.34884	475	1.42	0.23	10.4	13.0	40.4	36.2	16.7	0.0556	1386.82	5.73	0.100	44.14
25	43.15422	21.35422	428	1.28	1.08	31.5	34.2	24.8	9.6	69.4	0.0481	1537.47	1.92	0.100	14.22
26	43.03973	21.35578	458	0.91	1.57	9.4	23.8	12.9	53.9	28.1	0.0319	1398.72	4.05	0.004	0.72
27	43.26912	21.3638	324	1.09	0.63	36.9	38.8	12.4	11.9	68.3	0.0421	1463.61	0.13	0.100	0.81
28	43.34505	21.40109	637	1.29	0.74	18.6	43.8	12.4	25.2	27.4	0.0527	1414.62	2.96	0.004	0.88
29	43.22336	21.41132	283	1.27	0.45	30.7	47.5	15.9	6.0	70.4	0.0560	1396.45	2.10	0.100	16.42
30	43.04497	21.4114	641	1.41	0.52	11.9	27.3	19.9	40.9	20.4	0.0463	1434.48	3.42	0.004	0.91
31	43.28639	21.44564	390	1.15	1.30	25.8	49.4	15.2	9.6	33.5	0.0509	1400.85	0.34	0.100	2.41
32	42.99124	21.45765	1219	0.91	4.62	13.9	22.9	11.9	51.3	32.7	0.0155	1597.34	0.81	0.004	0.08
33	43.24868	21.49649	294	1.15	0.81	47.1	39.8	8.2	4.9	73.0	0.0408	1322.40	0.60	0.150	4.83
34	43.21364	21.49464	407	0.97	1.45	19.2	28.9	29.7	22.1	30.3	0.0492	1327.93	3.03	0.004	0.79
35	43.14908	21.55531	1081	1.11	4.59	17.9	28.5	16.6	37.0	13.9	0.0185	1686.57	0.41	0.004	0.05
36	43.33118	21.55507	520	1.04	0.53	14.0	28.4	29.3	28.4	42.1	0.0553	1356.09	2.75	0.004	0.82
37	43.19335	21.56225	556	1.28	1.29	14.6	29.1	12.4	44.0	34.1	0.0354	1370.14	3.04	0.004	0.59
38	43.28377	21.56974	383	1.45	0.14	18.3	28.2	35.3	18.3	34.2	0.0611	1324.27	0.93	0.100	7.51
39	43.2473	21.58936	314	0.98	0.38	26.5	25.3	20.5	27.7	47.9	0.0448	1236.84	0.71	0.004	0.16
40	43.19727	21.62386	466	1.27	2.45	17.0	30.4	13.8	38.8	16.7	0.0302	1318.13	4.27	0.100	16.99
41	43.21549	21.65258	224	1.44	0.67	25.6	42.7	26.1	5.6	35.2	0.0550	1265.90	0.00	0.150	0.00
42	43.14349	21.65991	635	1.14	0.78	9.0	11.5	28.1	51.4	24.5	0.0387	1448.11	2.21	0.004	0.50
43	43.17827	21.70494	260	1.36	0.67	31.5	32.7	14.1	21.7	41.6	0.0416	1317.13	1.42	0.150	11.69
44	43.11233	21.70848	309	1.44	2.26	25.6	35.4	15.3	23.8	38.5	0.0353	1377.55	0.56	0.100	2.71
45	43.17419	21.75485	253	1.3	4.66	35.6	42.7	10.5	11.1	50.0	0.0236	1358.42	1.65	0.150	7.94
46	43.22147	21.75931	276	1.42	1.31	34.4	22.4	14.4	28.8	45.7	0.0312	1312.09	0.52	0.150	3.18

Appendix B

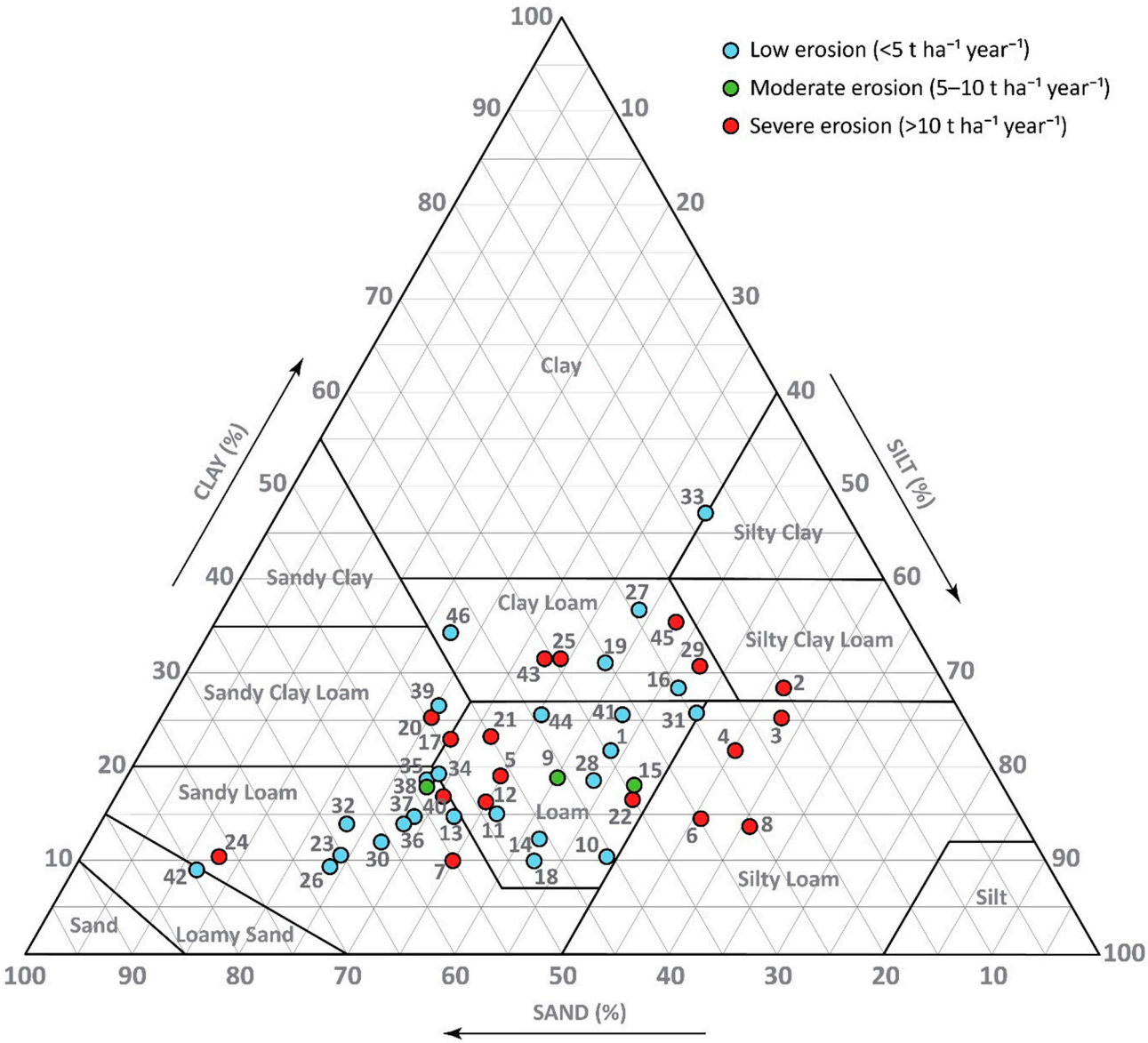


Figure A1. USDA textural classification of samples, colored by EU erosion severity classes.

Appendix C

Table A2. Point-based descriptive statistics of erosion rates across elevation classes.

Variable	Elevation (m)	Mean *	SE Mean	Coef. Var.	Min.	Median	Max.	Skewness	Kurtosis
Erosion rate	200–550	8.80 ^{A}	2.05	123.26	0.00	3.09	44.14	1.71	3.07
	550–900	14.19 ^{A}	5.31	129.53	0.50	3.87	45.12	1.01	−0.92
	900–1250	24.4 ^{A}	14.3	143.60	0.1	9.1	89.3	1.64	2.38

* No significant differences between the classes were detected according to one-way ANOVA (analysis of variance) followed by Tukey's HSD (Honestly Significant Difference) test ($p < 0.05$).

References

1. Pretty, J.; Bharucha, Z.P. Sustainable intensification in agricultural systems. *Ann. Bot.* **2014**, *114*, 1571–1596. [CrossRef]
2. Amundson, R.; Berhe, A.A.; Hopmans, J.W.; Olson, C.; Sztein, A.E.; Sparks, D.L. Soil and human security in the 21st century. *Science* **2015**, *348*, 1261071. [CrossRef] [PubMed]

3. Chartres, C.J.; Noble, A. Sustainable intensification: Overcoming land and water constraints on food production. *Food Secur.* **2015**, *7*, 235–245. [CrossRef]
4. Lewandowski, A.M.; Cates, A. Connecting soil health and water quality in agricultural landscapes. *J. Environ. Qual.* **2023**, *52*, 412–421. [CrossRef]
5. Adhikari, K.; Hartemink, A.E. Linking soils to ecosystem services—A global review. *Geoderma* **2016**, *262*, 101–111. [CrossRef]
6. Keesstra, S.D.; Bouma, J.; Wallinga, J.; Tittonell, P.; Smith, P.; Cerdà, A.; Montanarella, L.; Quinton, J.N.; Pachepsky, Y.; van der Putten, W.H.; et al. The significance of soils and soil science towards realization of the United Nations Sustainable Development Goals. *SOIL* **2016**, *2*, 111–128. [CrossRef]
7. Telo Da Gama, J. The Role of Soils in Sustainability, Climate Change, and Ecosystem Services: Challenges and Opportunities. *Ecologies* **2023**, *4*, 552–567. [CrossRef]
8. Boardman, J.; Poesen, J. (Eds.) *Soil Erosion in Europe*, 1st ed.; Wiley: Hoboken, NJ, USA, 2006. [CrossRef]
9. Pimentel, D.; Burgess, M. Soil Erosion Threatens Food Production. *Agriculture* **2013**, *3*, 443–463. [CrossRef]
10. Bosco, C.; De Rigo, D.; Dewitte, O.; Poesen, J.; Panagos, P. Modelling soil erosion at European scale: Towards harmonization and reproducibility. *Nat. Hazards Earth Syst. Sci.* **2015**, *15*, 225–245. [CrossRef]
11. Steinhoff-Knopp, B.; Kuhn, T.K.; Burkhard, B. The impact of soil erosion on soil-related ecosystem services: Development and testing a scenario-based assessment approach. *Environ. Monit. Assess.* **2021**, *193*, 274. [CrossRef]
12. Galindo, V.; Giraldo, C.; Lavelle, P.; Armbrecht, I.; Fonte, S.J. Land use conversion to agriculture impacts biodiversity, erosion control, and key soil properties in an Andean watershed. *Ecosphere* **2022**, *13*, e3979. [CrossRef]
13. Pimentel, D. Soil Erosion: A Food and Environmental Threat. *Environ. Dev. Sustain.* **2006**, *8*, 119–137. [CrossRef]
14. Nearing, M.A.; Xie, Y.; Liu, B.; Ye, Y. Natural and anthropogenic rates of soil erosion. *Int. Soil Water Conserv. Res.* **2017**, *5*, 77–84. [CrossRef]
15. Shojaeezadeh, S.A.; Al-Wardy, M.; Nikoo, M.R.; Mooselu, M.G.; Alizadeh, M.R.; Adamowski, J.F.; Moradkhani, H.; Alamdari, N.; Gandomi, A.H. Soil erosion in the United States: Present and future (2020–2050). *Catena* **2024**, *242*, 108074. [CrossRef]
16. Borrelli, P.; Robinson, D.A.; Fleischer, L.R.; Lugato, E.; Ballabio, C.; Alewell, C.; Meusburger, K.; Modugno, S.; Schütt, B.; Ferro, V.; et al. An assessment of the global impact of 21st century land use change on soil erosion. *Nat. Commun.* **2017**, *8*, 2013. [CrossRef] [PubMed]
17. Ananda, J.; Herath, G. Soil erosion in developing countries: A socio-economic appraisal. *J. Environ. Manag.* **2003**, *68*, 343–353. [CrossRef] [PubMed]
18. Kodiwo, M.O.; Otieno, C.A.; Ang, F. Socio-demographic Determinants of Soil Erosion Levels among the Farming Households in Nyakach Sub-county, Kenya. *IOSR J. Humanit. Soc. Sci.* **2019**, *24*, 12–21.
19. Walsh, K.; Berger, J.-F.; Roberts, C.N.; Vanniere, B.; Ghilardi, M.; Brown, A.G.; Woodbridge, J.; Lespez, L.; Estrany, J.; Glais, A.; et al. Holocene demographic fluctuations, climate and erosion in the Mediterranean: A meta data-analysis. *Holocene* **2019**, *29*, 864–885. [CrossRef]
20. Wynants, M.; Kelly, C.; Mtei, K.; Munishi, L.; Patrick, A.; Rabinovich, A.; Nasseri, M.; Gilvear, D.; Roberts, N.; Boeckx, P.; et al. Drivers of increased soil erosion in East Africa's agro-pastoral systems: Changing interactions between the social, economic and natural domains. *Reg. Environ. Change* **2019**, *19*, 1909–1921. [CrossRef]
21. Tošić, R.; Lovrić, N.; Dragićević, S. Assessment of the impact of depopulation on soil erosion: Case study—Republika Srpska (Bosnia and Herzegovina). *Carpathian J. Earth Environ. Sci.* **2019**, *14*, 505–518. [CrossRef]
22. Gocić, M.; Dragićević, S.; Radivojević, A.; Martić Bursać, N.; Stričević, L.; Đorđević, M. Changes in Soil Erosion Intensity Caused by Land Use and Demographic Changes in the Jablanica River Basin, Serbia. *Agriculture* **2020**, *10*, 345. [CrossRef]
23. Huang, L.; Ye, A.; Tang, C.; Duan, Q.; Zhang, Y. Impact of rural depopulation and climate change on vegetation, runoff and sediment load in the Gan River basin, China. *Hydrol. Res.* **2020**, *51*, 768–780. [CrossRef]
24. Petrović, A.M.; Manojlović, S.; Srejić, T.; Zlatanović, N. Insights into Land-Use and Demographical Changes: Runoff and Erosion Modifications in the Highlands of Serbia. *Land* **2024**, *13*, 1342. [CrossRef]
25. Stathopoulos, N.; Lykoudi, E.; Vasileiou, E.; Rozos, D.; Dimitrakopoulos, D. Erosion Vulnerability Assessment of Sperchios River Basin, in East Central Greece—A GIS Based Analysis. *Open J. Geol.* **2017**, *7*, 621–646. [CrossRef]
26. Borrelli, P.; Alewell, C.; Alvarez, P.; Anache, J.A.A.; Baartman, J.; Ballabio, C.; Bezak, N.; Biddoccu, M.; Cerdà, A.; Chalise, D.; et al. Soil erosion modelling: A global review and statistical analysis. *Sci. Total Environ.* **2021**, *780*, 146494. [CrossRef] [PubMed]
27. Bueno-Hurtado, P.; Seidou, O. Empirical and physical modelling of soil erosion in agricultural hillslopes. *J. Hydrol. Hydromech.* **2024**, *72*, 279–291. [CrossRef]
28. Gericke, A. Soil loss estimation and empirical relationships for sediment delivery ratios of European river catchments. *Int. J. River Basin Manag.* **2015**, *13*, 179–202. [CrossRef]
29. Jakubínský, J.; Pechanec, V.; Procházka, J.; Cudlín, P. Modelling of Soil Erosion and Accumulation in an Agricultural Landscape—A Comparison of Selected Approaches Applied at the Small Stream Basin Level in the Czech Republic. *Water* **2019**, *11*, 404. [CrossRef]

30. Wischmeier, W.H.; Smith, D.D. Predicting Rainfall Erosion Losses: A Guide to Conservation Planning. In *Agriculture Handbook, No. 537. US Department of Agriculture*; United States Department of Agriculture: Washington, DC, USA, 1978. Available online: https://www.ars.usda.gov/ARSUserFiles/60600505/RUSLE/AH_537%20Predicting%20Rainfall%20Soil%20Losses.pdf (accessed on 1 February 2026).
31. Renard, K.; Foster, G.; Weesies, G.; McCool, D.; Yoder, D. Predicting Soil Erosion by Water: A Guide to Conservation Planning with the Revised Universal Soil Loss Equation (RUSLE). In *Agriculture Handbook*; No. 703; US Department of Agriculture: Washington, DC, USA, 1997. Available online: https://www.tucson.ars.ag.gov/unit/publications/PDFfiles/717.pdf (accessed on 1 February 2026).
32. Pandey, S.; Kumar, P.; Zlatic, M.; Nautiyal, R.; Panwar, V.P. Recent advances in assessment of soil erosion vulnerability in a watershed. *Int. Soil Water Conserv. Res.* **2021**, *9*, 305–318. [CrossRef]
33. Benavidez, R.; Jackson, B.; Maxwell, D.; Norton, K. A review of the (Revised) Universal Soil Loss Equation ((R)USLE): With a view to increasing its global applicability and improving soil loss estimates. *Hydrol. Earth Syst. Sci.* **2018**, *22*, 6059–6086. [CrossRef]
34. Alewell, C.; Borrelli, P.; Meusburger, K.; Panagos, P. Using the USLE: Chances, challenges and limitations of soil erosion modelling. *Int. Soil Water Conserv. Res.* **2019**, *7*, 203–225. [CrossRef]
35. Kumar, R.; Deshmukh, B.; Kumar, A. Using Google Earth Engine and GIS for basin scale soil erosion risk assessment: A case study of Chambal river basin, central India. *J. Earth Syst. Sci.* **2022**, *131*, 228. [CrossRef]
36. Wang, H.; Zhao, H. Dynamic Changes of Soil Erosion in the Taohe River Basin Using the RUSLE Model and Google Earth Engine. *Water* **2020**, *12*, 1293. [CrossRef]
37. Dutta, D.; Das, S.; Kundu, A.; Taj, A. Soil erosion risk assessment in Sanjal watershed, Jharkhand (India) using geo-informatics, RUSLE model and TRMM data. *Model. Earth Syst. Environ.* **2015**, *1*, 37. [CrossRef]
38. Perović, V.; Životić, L.; Kadović, R.; Đorđević, A.; Jaramaz, D.; Mrvić, V.; Todorović, M. Spatial modelling of soil erosion potential in a mountainous watershed of South-eastern Serbia. *Environ. Earth Sci.* **2013**, *68*, 115–128. [CrossRef]
39. Panagos, P.; Borrelli, P.; Poesen, J.; Ballabio, C.; Lugato, E.; Meusburger, K.; Montanarella, L.; Alewell, C. The new assessment of soil loss by water erosion in Europe. *Environ. Sci. Policy* **2015**, *54*, 438–447. [CrossRef]
40. Marcinkowski, P.; Szporak-Wasilewska, S.; Kardel, I. Assessment of soil erosion under long-term projections of climate change in Poland. *J. Hydrol.* **2022**, *607*, 127468. [CrossRef]
41. European Commission; Joint Research Centre; European Environment Agency. *The State of Soils in Europe: Fully Evidenced, Spatially Organised Assessment of the Pressures Driving Soil Degradation*; Publications Office: Luxembourg, 2024; Available online: https://data.europa.eu/doi/10.2760/7007291 (accessed on 24 October 2025).
42. Panagos, P.; Ballabio, C.; Poesen, J.; Lugato, E.; Scarpa, S.; Montanarella, L.; Borrelli, P. A Soil Erosion Indicator for Supporting Agricultural, Environmental and Climate Policies in the European Union. *Remote Sens.* **2020**, *12*, 1365. [CrossRef]
43. Milentijević, N.; Ostojić, M.; Fekete, R.; Kalkan, K.; Ristić, D.; Bačević, N.; Stevanović, V.; Pantelić, M. Assessment of Soil Erosion Rates Using RevisedUniversal Soil Loss Equation (RUSLE)and GIS in Bačka (Serbia). *Pol. J. Environ. Stud.* **2021**, *30*, 5175–5184. [CrossRef]
44. Belanovic, S.; Perovic, V.; Vidojevic, D.; Kostadinov, S.; Knezevic, M.; Kadovic, R.; Košanin, O. Assessment of soil erosion intensity in Kolubara District, Serbia. *Fresenius Environ. Bull.* **2013**, *22*, 1556–1563.
45. Čupić, A.; Smičiklas, I.; Manić, M.; Đokić, M.; Dragović, R.; Đorđević, M.; Gocić, M.; Jović, M.; Topalović, D.; Gajić, B.; et al. ^{137}Cs-Based Assessment of Soil Erosion Rates in a Morphologically Diverse Catchment with Varying Soil Types and Vegetation Cover: Relationship with Soil Properties and RUSLE Model Predictions. *Water* **2025**, *17*, 526. [CrossRef]
46. Perović, V.; Dordević, A.; Životić, L.; Nikolić, N.; Kadović, R.; Belanović, S. Soil erosion modelling in the complex terrain of Pirot municipality. *Carpathian J. Earth Environ. Sci.* **2012**, *7*, 93–100.
47. Perovic, V.; Jaramaz, D.; Zivotic, L.; Cakmak, D.; Mrvic, V.; Milanovic, M.; Saljnikov, E. Design and implementation of WebGIS technologies in evaluation of erosion intensity in the municipality of NIS (Serbia). *Environ. Earth Sci.* **2016**, *75*, 211. [CrossRef]
48. Životić, L.; Perović, V.; Jaramaz, D.; Dordević, A.; Petrović, R.; Todorović, M. Application of USLE, GIS, and Remote Sensing in the Assessment of Soil Erosion Rates in Southeastern Serbia. *Pol. J. Environ. Stud.* **2012**, *21*, 1929–1935.
49. Tošić, R.; Dragićević, S.; Kostadinov, S.; Dragović, N. Assessment of soil erosion potential by the USLE method: Case study, Republic of Srpska—BiH. *Fresenius Environ. Bull.* **2011**, *20*, 1910–1917.
50. Patriche, C.V. Applying RUSLE for soil erosion estimation in Romania under current and future climate scenarios. *Geoderma Reg.* **2023**, *34*, e00687. [CrossRef]
51. Kostadinov, S.; Dragović, N.; Janković, S.; Tošić, R. The impact of anti-erosion works in the Toplica River Basin upstream of the "Selova" dam on soil erosion intensity. *Vodoprivreda* **2008**, *40*, 115–126.
52. ESDAC. European Soil Data Centre. 2024. Available online: https://esdac.jrc.ec.europa.eu/resource-type/datasets (accessed on 22 March 2025).

53. Institute for Nature Conservation of Serbia. National Park Kopaonik. Available online: https://zzps.rs/%D0%BD%D0%B0%D1%86%D0%B8%D0%BE%D0%BD%D0%B0%D0%BB%D0%BD%D0%B8-%D0%BF%D0%B0%D1%80%D0%BA-%D0%BA%D0%BE%D0%BF%D0%B0%D0%BE%D0%BD%D0%B8%D0%BA/ (accessed on 26 October 2025).
54. Lakušić, D.; Ranđelović, V. Review of plant communities of Mt. Kopaonik (SW Serbia, Yugoslavia). *Ekologija* **1996**, *31*, 1–16.
55. Republic Hydrometeorological Service of Serbia—RHMZ. Hydrological Yearbooks. Available online: https://www.hidmet.gov.rs/ciril/hidrologija/povrsinske_godisnjaci.php (accessed on 27 October 2025).
56. *ISO 11272:2017*; Soil Quality. Determination of Dry Bulk Density. International Organization for Standardization: Geneva, Switzerland, 2017. Available online: https://www.iso.org/standard/68255.html (accessed on 27 October 2025).
57. *ISO 11277:2020*; Soil Quality—Determination of Particle Size Distribution in Mineral Soil Material—Method by Sieving and Sedimentation. International Organization for Standardization: Geneva, Switzerland, 2020. Available online: https://www.iso.org/standard/69496.html (accessed on 27 October 2025).
58. *ISO 14235:1998*; Soil Quality—Determination of Organic Carbon by Sulfochromic Oxidation. International Organization for Standardization: Geneva, Switzerland, 1998. Available online: https://www.iso.org/standard/23140.html (accessed on 27 October 2025).
59. *ISO 11465:1993*; Soil Quality—Determination of Dry Matter and Water Content on A Mass Basis—Gravimetric Method. International Organization for Standardization: Geneva, Switzerland, 1993. Available online: https://www.iso.org/standard/20886.html (accessed on 17 March 2025).
60. Godoi, R.D.F.; Rodrigues, D.B.B.; Borrelli, P.; Oliveira, P.T.S. High-resolution soil erodibility map of Brazil. *Sci. Total Environ.* **2021**, *781*, 146673. [CrossRef]
61. *World Reference Base for Soil Resources 2022: International Soil Classification System for Naming Soils and Creating Legends for Soil Maps*, 4th ed.; International Union of Soil Sciences: Vienna, Austria, 2022.
62. *National Soil Survey Handbook*; The U.S. Department of Agriculture, Natural Resources Conservation Service (NRCS): Washington, DC, USA, 1983. Available online: https://directives.nrcs.usda.gov/sites/default/files2/1719847021/National%20Soil%20Survey%20Handbook%20%28entire%20handbook%29.pdf (accessed on 27 October 2025).
63. Xu, Y.-Q.; Shao, X.M.; Kong, X.B.; Peng, J.; Cai, Y.-L. Adapting the RUSLE and GIS to model soil erosion risk in a mountains karst watershed, Guizhou Province, China. *Environ. Monit. Assess.* **2008**, *141*, 275–286. [CrossRef]
64. Sekulić, A.; Kilibarda, M.; Protić, D.; Bajat, B. A high-resolution daily gridded meteorological dataset for Serbia made by Random Forest Spatial Interpolation. *Sci. Data* **2021**, *8*, 123. [CrossRef]
65. Arnoldus, H.M.J. FAO Soil Bulletin 34 Assessing Soil Degradation: Methodology Used to Determine the Maximum Average Soil Loss Due to Sheet and Rill Erosion in Morocco, Rome. 1977. Available online: https://www.fao.org/3/ar114e/ar114e.pdf (accessed on 22 March 2025).
66. Chen, W.; Huang, Y.-C.; Lebar, K.; Bezak, N. A systematic review of the incorrect use of an empirical equation for the estimation of the rainfall erosivity around the globe. *Earth-Sci. Rev.* **2023**, *238*, 104339. [CrossRef]
67. Ghosal, K.; Das Bhattacharya, S. A Review of RUSLE Model. *J. Indian Soc. Remote Sens.* **2020**, *48*, 689–707. [CrossRef]
68. Schmidt, S.; Tresch, S.; Meusburger, K. Modification of the RUSLE slope length and steepness factor (LS-factor) based on rainfall experiments at steep alpine grasslands. *MethodsX* **2019**, *6*, 219–229. [CrossRef]
69. Ganasri, B.P.; Ramesh, H. Assessment of soil erosion by RUSLE model using remote sensing and GIS—A case study of Nethravathi Basin. *Geosci. Front.* **2016**, *7*, 953–961. [CrossRef]
70. Allafta, H.; Opp, C. Soil Erosion Assessment Using the RUSLE Model, Remote Sensing, and GIS in the Shatt Al-Arab Basin (Iraq-Iran). *Appl. Sci.* **2022**, *12*, 7776. [CrossRef]
71. NASA JPL. *NASA Shuttle Radar Topography Mission Global 1 Arc Second*; NASA Land Processes Distributed Active Archive Center: Sioux Falls, SD, USA, 2013. [CrossRef]
72. Wang, L.; Liu, H. An efficient method for identifying and filling surface depressions in digital elevation models for hydrologic analysis and modelling. *Int. J. Geogr. Inf. Sci.* **2006**, *20*, 193–213. [CrossRef]
73. Moore, I.D.; Grayson, R.B.; Ladson, A.R. Digital terrain modelling: A review of hydrological, geomorphological, and biological applications. *Hydrol. Process.* **1991**, *5*, 3–30. [CrossRef]
74. Efthimiou, N.; Lykoudi, E.; Karavitis, C. Soil erosion assessment using the RUSLE model and GIS. *Eur. Water* **2014**, *47*, 15–30.
75. Rozos, D.; Skilodimou, H.D.; Loupasakis, C.; Bathrellos, G.D. Application of the revised universal soil loss equation model on landslide prevention. An example from N. Euboea (Evia) Island, Greece. *Environ. Earth Sci.* **2013**, *70*, 3255–3266. [CrossRef]
76. Zanaga, D.; Van De Kerchove, R.; De Keersmaecker, W.; Souverijns, N.; Brockmann, C.; Quast, R.; Wevers, J.; Grosu, A.; Paccini, A.; Vergnaud, S.; et al. *ESA WorldCover 10 m 2020 v100 2021*; Zenodo: Geneva, Switzerland, 2001. [CrossRef]
77. Chen, P. Assessment of soil loss from land use/land cover change and disasters in the Longmen Shan Mountains, China. *Appl. Ecol. Environ. Res.* **2019**, *17*, 11233–11247. [CrossRef]

78. Kuok, K.K.K.; Mah, D.Y.S.; Chiu, P.C. Evaluation of C and P Factors in Universal Soil Loss Equation on Trapping Sediment: Case Study of Santubong River. *J. Water Resour. Prot.* **2013**, *5*, 1149–1154. [CrossRef]
79. Lu, H.; Prosser, I.P.; Moran, C.J.; Gallant, J.C.; Priestley, G.; Stevenson, J.G. Predicting sheetwash and rill erosion over the Australian continent. *Soil Res.* **2003**, *41*, 1037–1062. [CrossRef]
80. Svorin, J. A test of three soil erosion models incorporated into a geographical information system. *Hydrol. Process.* **2003**, *17*, 967–977. [CrossRef]
81. Sulistyo, B.; Gunawan, T.; Hartono, H.; Danoedoro, P. Toward A Fully and Absolutely Raster-Based Erosion Modeling By Using RS and GIS. *Indones. J. Geogr.* **2009**, *41*, 149–170.
82. Martínez-Graña, A.; Carrillo, J.; Lombana, L.; Criado, M.; Palacios, C. Mapping the Risk of Water Soil Erosion in Larrodrigo (Salamanca, Spain) Using the RUSLE Model and A-DInSAR Technique. *Agronomy* **2021**, *11*, 2120. [CrossRef]
83. Alsafadi, K.; Bi, S.; Abdo, H.G.; Al Sayah, M.J.; Ratonyi, T.; Harsanyi, E.; Mohammed, S. Spatial–temporal dynamic impact of changes in rainfall erosivity and vegetation coverage on soil erosion in the Eastern Mediterranean. *Environ. Sci. Pollut. Res.* **2022**, *31*, 40511–40529. [CrossRef]
84. Sachapara, N.; Patel, M.; Dhameliya, H.; Jodhani, K.; Gupta, N.; Patel, D.; Singh, S.K. Dynamic Flood and Erosion Modeling for the Sabarmati River Using RUSLE and GEE. Available online: https://meetingorganizer.copernicus.org/EGU25/EGU25-664.html (accessed on 24 October 2025).
85. QGIS Development Team. QGIS Geographic Information System. 2025. Available online: http://qgis.org (accessed on 2 October 2025).
86. Conrad, O.; Bechtel, B.; Bock, M.; Dietrich, H.; Fischer, E.; Gerlitz, L.; Wehberg, J.; Wichmann, V.; Böhner, J. System for Automated Geoscientific Analyses (SAGA) v. 2.1.4. *Geosci. Model Dev.* **2015**, *8*, 1991–2007. [CrossRef]
87. Shapiro, S.S.; Wilk, M.B. An analysis of variance test for normality (complete samples). *Biometrika* **1965**, *52*, 591–611. [CrossRef]
88. *Microsoft Excel*; Microsoft Corporation: Redmond, WA, USA, 2024; Available online: https://www.microsoft.com/ (accessed on 1 February 2026).
89. Ducić, V.; Radovanović, M. *Climate of Serbia*; Institute for Textbooks and Teaching Aids: Belgrade, Serbia, 2005.
90. Stanojevic, G. Analysis of annual sums of precipitation in Serbia. *J. Geogr. Inst. Jovan Cvijic SASA* **2012**, *62*, 1–13. [CrossRef]
91. Živković, N.; Anđelković, G. Altitude Precipitation Gradient in Serbia. *Bull. Serbian Geogr. Soc.* **2024**, *84*, 31–36. Available online: https://scispace.com/pdf/altitude-precipitation-gradient-in-serbia-2fn5plvxbh.pdf (accessed on 28 October 2025).
92. Živković, N. *Average Annual and Seasonal River Runoff in Serbia*; Faculty of Geography, University of Belgrade: Belgrade, Serbia, 2009.
93. Golijanin, J.; Nikolić, G.; Valjarević, A.; Ivanović, R.; Tunguz, V.; Bojić, S.; Grmuša, M.; Lukić Tanović, M.; Perić, M.; Hrelja, E.; et al. Estimation of potential soil erosion reduction using GIS-based RUSLE under different land cover management models: A case study of Pale Municipality, B&H. *Front. Environ. Sci.* **2022**, *10*, 945789. [CrossRef]
94. Tošić, R.; Kapović, M.; Lovrić, N.; Dragićević, S. Assessment of soil erosion potential using RUSLE and GIS. *Fresenius Environ. Bull.* **2013**, *22*, 3415–3423.
95. Kouli, M.; Soupios, P.; Vallianatos, F. Soil erosion prediction using the Revised Universal Soil Loss Equation (RUSLE) in a GIS framework, Chania, Northwestern Crete, Greece. *Environ. Geol.* **2009**, *57*, 483–497. [CrossRef]
96. Thakuriah, G. GIS-based revised universal soil loss equation for estimating annual soil erosion: A case of lower Kulsi basin, India. *SN Appl. Sci.* **2023**, *5*, 81. [CrossRef]
97. Eurostat Agri-Environmental Indicator—Soil Erosion. 2020. Available online: https://ec.europa.eu/eurostat/statistics-explained/index.php?title=Agri-environmental_indicator_-_soil_erosion (accessed on 22 March 2025).
98. Kostadinov, S.; Braunović, S.; Dragićević, S.; Zlatić, M.; Dragović, N.; Rakonjac, N. Effects of Erosion Control Works: Case Study—Grdelica Gorge, the South Morava River (Serbia). *Water* **2018**, *10*, 1094. [CrossRef]
99. Stefanović, I.; Ristić, R.; Dragović, N.; Stefanović, M.; Živanović, N.; Čotrić, J. Effects of Erosion Control Works: Case Study–Reservoir Celije, Rasina River Basin, the Zapadna Morava River (Serbia). *Water* **2024**, *16*, 855. [CrossRef]
100. Li, P.; Xie, Z.; Yan, Z.; Dong, R.; Tang, L. Assessment of vegetation restoration impacts on soil erosion control services based on a biogeochemical model and RUSLE. *J. Hydrol. Reg. Stud.* **2024**, *53*, 101830. [CrossRef]
101. Sittig, S.; Sur, R. Runoff and erosion mitigation via conservation tillage and cover crops—Derivation of model input parameters from literature. *Environ. Chall.* **2024**, *17*, 101015. [CrossRef]
102. Ahmad, N.S.; Mustafa, F.B.; Didams, G. A systematic review of soil erosion control practices on the agricultural land in Asia. *Int. Soil Water Conserv. Res.* **2020**, *8*, 103–115. [CrossRef]
103. Yang, R.; Yang, S.; Chen, L.; Yang, Z.; Xu, L.; Zhang, X.; Liu, G.; Zhang, X.; Jiao, C.; Bai, R.; et al. Effect of vegetation restoration on soil erosion control and soil carbon and nitrogen dynamics: A meta-analysis. *Soil Tillage Res.* **2023**, *230*, 105705. [CrossRef]
104. Thiengo, C.C.; De Souza, G.S.; Algarin, C.A.V.; Da Silva, D.M.N.; De Sá Mendonça, E. Effects of soil tillage practices on soil conservation in pasture-based integrated management systems: A case study on steep slopes in southeastern Brazil. *Discov. Soil* **2024**, *1*, 26. [CrossRef]

105. Feeney, C.J.; Robinson, D.A.; Thomas, A.R.C.; Borrelli, P.; Cooper, D.M.; May, L. Agricultural practices drive elevated rates of topsoil decline across Kenya, but terracing and reduced tillage can reverse this. *Sci. Total Environ.* **2023**, *870*, 161925. [CrossRef]
106. Mejía-Parada, C.; Mora-Ruiz, V.; Vallejo-Borda, J.A.; Arrieta-Baldovino, J. Influence of LS Factor Overestimation Soil Loss on RUSLE Model for Complex Topographies. *J. Indian Soc. Remote Sens.* **2024**, *52*, 1661–1674. [CrossRef]

Disclaimer/Publisher's Note: The statements, opinions and data contained in all publications are solely those of the individual author(s) and contributor(s) and not of MDPI and/or the editor(s). MDPI and/or the editor(s) disclaim responsibility for any injury to people or property resulting from any ideas, methods, instructions or products referred to in the content.